MALLMANN, GUILHERME; FONSECA, RAÚL O. C.; SILVA, ADOLFO B.

An experimental study of the partitioning of trace elements between rutile and silicate melt as a function of oxygen fugacity

An experimental study of the partitioning of trace elements between rutile and silicate melt as a function of oxygen fugacity

GUILHERME MALLMANN[1,4], RAÚL O.C. FONSECA[2] and ADOLFO B. SILVA[3]

[1]Instituto de Geociências, Universidade de São Paulo, Rua do Lago, 562,
Cidade Universitária, 05508-080 São Paulo, SP, Brasil

[2]Steinmann Institut für Geologie, Mineralogie und Paleontologie,
Universität Bonn, Poppelsdorfer Schloss, Bonn, 53115, Germany

[3]Instituto de Astronomia, Geofísica e Ciências Atmosféricas, Universidade de São Paulo,
Rua do Matão, 1226, Cidade Universitária, 05508-090 São Paulo SP, Brasil

[4]School of Earth Sciences, The University of Queensland, Brisbane, QDL 4072, Australia

ABSTRACT

Subduction zone or arc magmas are known to display a characteristic depletion of High Field Strength Elements (HFSE) relative to other similarly incompatible elements, which can be attributed to the presence of the accessory mineral rutile (TiO_2) in the residual slab. Here we show that the partitioning behavior of vanadium between rutile and silicate melt varies from incompatible (~0.1) to compatible (~18) as a function of oxygen fugacity. We also confirm that the HFSE are compatible in rutile, with D(Ta) > D(Nb) >> (D(Hf) >/~ D(Zr)), but that the level of compatibility is strongly dependent on melt composition, with partition coefficients increasing about one order of magnitude with increasing melt polymerization (or decreasing basicity). Our partitioning results also indicate that residual rutile may fractionate U from Th due to the contrasting (over 2 orders of magnitude) partitioning between these two elements. We confirm that, in addition to the HFSE, Cr, Cu, Zn and W are compatible in rutile at all oxygen fugacity conditions.

Key words: arc magma, HFSE, partition coefficient, redox, rutile.

INTRODUCTION

Despite their similar compatibility during mantle melting, the High Field Strength Elements (HFSE: Nb, Ta, Zr and Hf) display a characteristic depletion relative to the Rare Earth (REE) and Large Ion Lithophile (LILE) elements in subduction-related or arc magmas (see Tatsumi and Eggins 1995). In fact, this geochemical signature has long been used as a distinctive feature of arc magmas, yet its reason

remains controversial. Some authors argue that HFSEs are less mobile than LILEs and REEs and that, because of this, fluids produced by slab dehydration are depleted in these elements (e.g. McCulloch and Gamble 1991, Keppler 1996). However, recent experimental evidence indicates that the mobility of HFSEs during slab dehydration may approach that of light REEs and LILEs at increasing pressures and salute contents of fluids, which would then require the presence of a residual phase in the sources of arc magmas that could selectively retain

Correspondence to: Guilherme Mallmann
E-mail: guil.mallmann@gmail.com

the HFSEs to explain their depletion (e.g. Brenan et al. 1995, Stalder et al. 1998, Ionov and Hofmann 1995, Tiepolo et al. 2000).

Rutile (TiO_2) is considered the prime candidate to retain HFSEs in residual subducted slabs since it has been shown to be a ubiquitous accessory phase in eclogites (e.g. Rudnick et al. 2000, Zack et al. 2002) and to incorporate large amounts of HFSEs (Green and Pearson 1987, Zack et al. 2002). Experimental studies have demonstrated that HFSEs are indeed compatible in rutile, but their partitioning behavior appears to be strongly dependent on melt composition (Horgn and Hess 2000, Klemme et al. 2005). In principle, the partitioning of HFSEs between rutile and silicate melt may also be influenced by the presence of other trace-element cations, which can either compete for crystallographic sites and/or allow for coupled substitution mechanisms such as $M^{2+} + M^{5+} = Ti^{4+} + M^{3+}$, or $M^{2+} + 2 M^{5+} = 3 Ti^{4+}$, or $4 M^{5+} + [\ ] = 5 Ti^{4+}$; where M^{x+} is a metal cation of specified valence and [ ] is a vacancy (Horng and Hess 2000).

Vanadium is a multivalent element which can occur as V^{2+}, V^{3+}, V^{4+} and V^{5+}, depending on oxygen fugacity (fO_2), in geological settings (e.g. Mallmann and O'Neill 2009, 2013). In its quadrivalent and pentavalent states, vanadium shows the same geochemical characteristic that defines the HFSEs, which is high ionic charge/ionic radius ratio. Hence, at appropriate redox conditions, vanadium should behave similarly to the HFSEs. Interestingly, the transition between the various vanadium valence states occurs over the range of oxygen fugacities inferred for the genesis of terrestrial magmas. Assuming that arc magmas are indeed formed under more oxidizing conditions than mid-ocean ridge and island arc magmas (e.g. Kelly and Cottrell 2009, Cottrell and Kelley 2011, Evans 2012), one would expect the partitioning behavior of V between rutile and silicate melt to vary considerably during the genesis of these different types of terrestrial magmas. To what extent the partitioning of

vanadium between rutile and silicate melt changes as a function of oxygen fugacity and, particularly, what is the indirect effect of changing oxygen fugacity (and vanadium partition coefficients) on the partitioning behavior of the homovalent HFSEs remains to be tested.

In this paper we report the results of an experimental study aimed at determining the effect of oxygen fugacity on the partitioning of trace elements between rutile and silicate melt. High temperature and pressure partitioning experiments were carried out over a range of oxygen fugacities (from 10^{-12} to $10^{+4.3}$ bars at 1300°C) sufficiently large to cover the transition from V^{3+} to V^{4+} to V^{5+} and, most importantly, the redox conditions inferred for terrestrial magmas.

MATERIALS AND METHODS

STARTING MATERIALS

We studied three compositions (SKHDAN1, SKHDRH1 and SM20), selected from the work of Klemme et al. 2005, which are known to equilibrate rutile and silicate melt at atmospheric pressure (1 bar) between 1250 and 1300°C (Table I). All compositions were prepared by combining appropriate amounts of reagent-grade oxides (SiO_2, TiO_2, Al_2O_3, MgO, Fe_2O_3) and carbonates ($CaCO_3$, Na_2CO_3 and K_2CO_3) to make 5 g of material. Composition SKHDAN1 was doped with 3 different cocktails of trace elements (to make 3 different starting materials labeled SKHDAN1-a, SKHDAN1-b, and SKHDAN1-c): the first containing 250-500 µg g^{-1} of the HFSEs Zr, Hf, Ta and Nb (i.e. only homovalent trace elements of valence 4+ and 5+); the second also containing, in addition to the HFSEs listed above, about 250-500 µg g^{-1} of V (a multivalent element); and the third containing 250-500 µg g^{-1} of several trace-element cations of various valence states, namely Zr, Hf, Ta, Nb, V, Th, Sc, U, Ga, Y, Fe, P, Cr, Li, Ni, Cu, Zn, Ba, Sr, Pb, In, Sb, Sn, Co, Ta, W. This last cocktail of trace elements was also added to compositions SKHDRH1 and SM20.

TABLE I
Starting compositions in cg/g.

	SKHDRH1	SKHDAN1	SM20
SiO_2	55.98	45.80	40.37
TiO_2	20.01	23.70	32.38
Al_2O_3	12.00	15.30	7.60
Na_2O	6.41	6.10	9.80
K_2O	5.60	3.10	1.55
CaO	---	6.00	2.31
MgO	---	---	1.90
FeO	---	---	4.09

ONE-ATMOSPHERE HIGH TEMPERATURE GAS-MIXING EXPERIMENTS

Charges for one-atmosphere (i.e. 1-bar) experiments were prepared by mixing about 100 mg of powder of each composition with a gel made from polyethylene oxide and water, and mounting the resulting sludge on either Pt or Re wire loops; the choice of wire depends on the target oxygen fugacity of a particular experiment (see Mallmann and O'Neill 2009). Five compositions were suspended together from a Pt "chandelier". The samples were introduced in the furnace at a temperature between 600 and 900°C (pre-conditioned with the desired gas mix). The temperature was then increased at a rate of 6°C min^{-1}

to 1425-1450°C. This temperature was maintained for 1 hour, and then slowly cooled at a rate of 6 to 12°C h^{-1} until the target equilibrium temperature of 1300°C had been reached. The slow cooling from the superliquidus temperature is necessary to minimize nucleation points and therefore grow fewer but larger crystals. Experiments were then held under these conditions for approximately 2 days and then dropped-quenched in water. All experiments were carried out in a GERO HRTV 70-250/18 vertical tube (high-purity 99.9% alumina) furnace at the Instituto de Geociências, Universidade de São Paulo, Brazil (Fig. 1). Gas flows were controlled by Aalborg mass flow controllers of 10, 100 and 200 SCCM calibrated for CO, CO_2 and O_2. Oxygen fugacity imposed by gas mixing was calculated using thermodynamic data compiled in Kress et al. (2004), and checked before starting the experimental campaign with a SIRO$_2$ C700+ solid zirconia electrolyte oxygen sensor. Results are shown in Fig. 2, and indicate accuracy better than 0.1 log fO_2 units. Temperature at the hot zone was checked with the help of a type B ($Pt_{70}Rh_{30}$-$Pt_{94}Rh_6$) thermocouple internal to the tube prior to the experiments. The furnace hotspot, identified via a temperature vertical profile, spans over 5cm
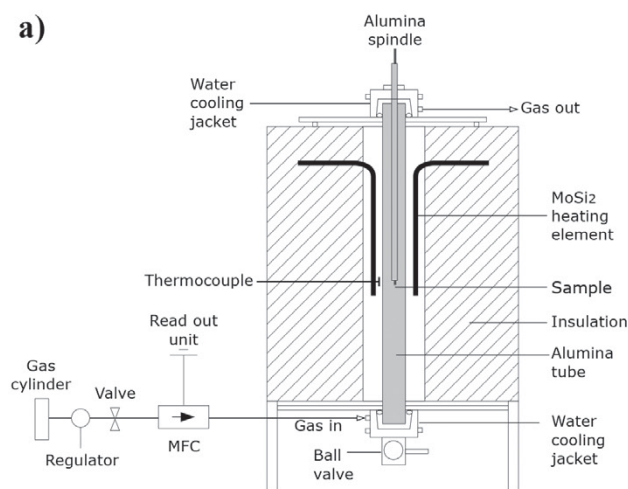

Figure 1 - Schematic drawing (a) and photograph (b) of the one-atmosphere vertical tube furnace with drop-quench mechanism and attached gas mixing system used in this study. MFC - mass flow controller.
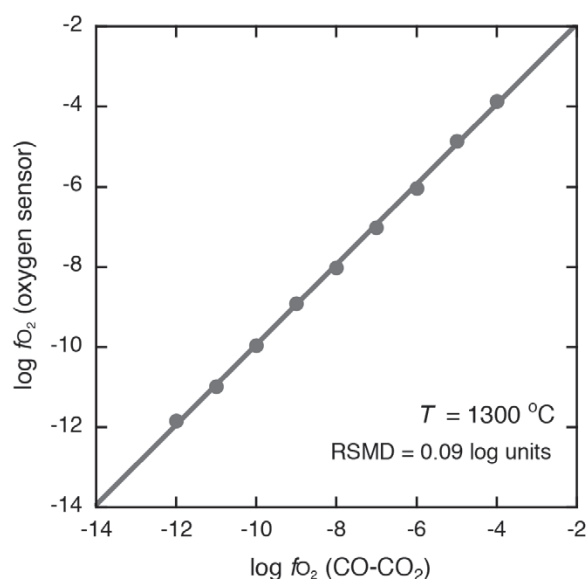
Figure 2 - Comparison between oxygen fugacity determined by CO-CO_2 gas mixing and measured by a SIRO$_2$ C700+ solid zirconia electrolyte oxygen sensor in the vertical tube furnace. All measurements were obtained at 1300°C (at the sensor) with air as reference. The root mean square deviation (RMSD) of the linear regression is 0.09 log units, which we take to roughly indicate the precision of the oxygen fugacity set by gas mixing.

vertically with temperature variability within ±2°C (Fig. 3). During the experiments, temperature was controlled by a type B thermocouple external to the muffle tube, feeding into a Eurotherm PID controller. A summary of experimental conditions is given in Table II.

HIGH PRESSURE AND TEMPERATURE PISTON-CYLINDER EXPERIMENTS

In order to achieve conditions more oxidizing than those accessible via pure O_2 gas at 1 bar, each of the 5 starting compositions were loaded into 2.3 mm Pt capsules along with PtO$_2$ and equilibrated at 1 GPa and 1300°C (Table II). Under the pressure and temperature conditions of these experiments, PtO$_2$ breaks down to Pt and sufficient O_2 to produce a partial pressure equal to the confining pressure, buffering the oxygen fugacity, which was calculated to be ~ $10^{+4.3}$ bars from the equation of state of pure O_2 given by Belonoshko

and Saxena (1991). The 5 capsules containing the samples and PtO$_2$ were placed inside a rod of crushable MgO, with interstitial spaces between the capsules filled with alumina cement. The MgO rod containing the 5 capsules was then placed inside a ¾" NaCl-Pyrex-graphite pressure assembly and equilibrated at pressure and temperature using a Bristol-type end-loaded piston cylinder apparatus housed at the Institute of Geosciences, University of São Paulo, Brazil (Fig. 4). Temperature was monitored using a type B thermocouple protected by high-purity alumina tubing. As for the 1-bar experiments, temperature was first raised above or near the liquidus and slowly cooled to the target temperature of 1300°C to promote the growth of fewer but larger crystals. After about 2 days at the equilibrium temperature, the experiment was quenched by switching off the power supply.

ANALYTICAL PROCEDURES

Recovered experimental charges were mounted in epoxy resin, grinded to expose the phases, polished, and then etched/cleaned for a few minutes in an ultrasonic bath with a dilute (1:10) solution of Citranox and distilled water in order to better reveal the crystals at the surface in reflected light. The major and trace element composition of experimental run products were analyzed by a JEOL JXA 8900 electron microprobe, and by a 193 nm Resonetics M50-E excimer laser ablation (LA) system coupled to a single collector quadrupole Thermo X-Series 2 mass spectrometer (ICP-MS), respectively. Both instruments are housed at the Steinmann Institut, Universität Bonn, Germany.

The crystalline phase present in all experimental samples was determined to be rutile after qualitative (EDS) electron microprobe spectral analyses, and further assumed to have a stoichiometric TiO$_2$ composition. Silicate melt quenched to glasses were analyzed by electron microprobe in WDS mode at 15 kV acceleration voltage, 10nA beam current and 10 micron beam diameter. Calibrations for Ca,

TABLE II
Experimental conditions.

Run	Type exp./ pressure	Wire loop/ capsule	T (°C) sup.	Duration (h) at sup.	Cooling rate (°C/h)	T (°C) eq.	Duration (h) at eq.	CO	Gas mix CO$_2$	O$_2$	log fO$_2$
								(% full scale x MFC range)			
SP280613	GMF / 1bar	Re	1450	1	6	1300	42	48.0x200	6.9x10	---	-14.0
SP040713	GMF / 1bar	Re	1450	1	6	1300	40	22.0x200	10.0x10	---	-13.0
SP070713	GMF / 1bar	Re	1450	1	6	1300	40	22.0x200	31.6x10	---	-12.0
SP220713	GMF / 1bar	Re	1450	1	6	1300	45	22.0x200	100.0x10	---	-11.0
SP300713	GMF / 1bar	Re	1450	1	6	1300	45	22.0x200	15.9x200	---	-10.0
SP070813	GMF / 1bar	Pt	1450	1	6	1300	40	9.6x200	22.0x200	---	-9.0
SP100813	GMF / 1bar	Pt	1450	1	6	1300	46	61.0x10	22.0x200	---	-8.0
SP050313	GMF / 1bar	Pt	1450	1	9	1300	36	19.2x10	22.0x200	---	-7.0
SP020313	GMF / 1bar	Pt	1450	1	9	1300	53	13.3x10	48.0x200	---	-6.0
SP270213	GMF / 1bar	Pt	1425	1	6	1300	45	4.2x10	48.0x200	---	-5.0
SP180213	GMF / 1bar	Pt	1425	1	12	1300	51	---	30.0x200	---	-3.4
SP130813	GMF / 1bar	Pt	1450	1	6	1300	43	---	30.0x200	---	-3.4
SP210213	GMF / 1bar	Pt	1425	1	12	1300	58	---	32.0x200	4.3x15§	-2.0
SP250713	GMF / 1bar	Pt	1450	1	6	1300	45	---	---	air*	-0.7
SP240213	GMF / 1bar	Pt	1425	1	12	1300	46	---	---	25.0x300	0.0
PC100813	PC / 1 GPa	Pt	1425	1	12	1300	48	---	---	---	4.3

GMF = gas mixing furnace, PC = piston cylinder. § MFC oscillating in the first 12 hours, then stable to 0.5%.

*Furnace open to air. ¶ Starting mixes loaded in Pt capsules with PtO$_2$.
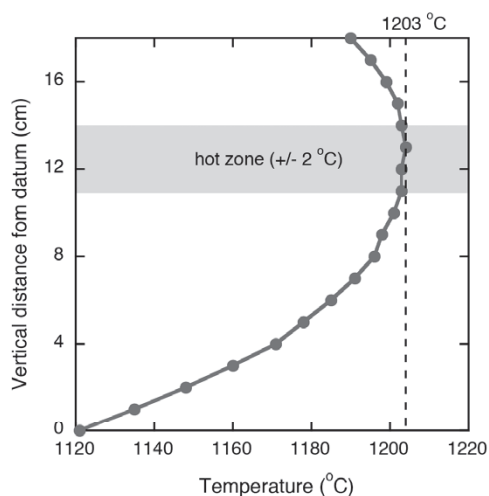

Figure 3 - Vertical temperature profile determined for the vertical tube furnace with a type B thermocouple placed inside the tube. All measurements were obtained at 1200°C (set by a type B thermocouple external to the tube) in air. All temperature values presented in the paper have been corrected for the 3°C offset between the internal and external thermocouples. Uncertainty in temperature is expected to be less than ±2°C at the hot zone.

Mg, Al, Si and Fe were obtained on BCR silicate glass standard, for Na on an in-house Jd-Di eutectic silicate glass, and for Ti on rutile. Accuracy and reproducibility were checked using the VG2 basaltic glass standard. The close to 100% totals obtained in all silicate glasses suggest that under the operation conditions Na loss was not an issue during analysis.

The trace element compositions of silicate glasses and rutile were determined by laser-ablation ICP-MS using the following isotopes: [7]Li, [23]Na, [24]Mg, [27]Al, [29]Si, ^{31}P, [39]K, [43]Ca, [45]Sc, [47]Ti, [51]V, [52]Cr, [55]Mn, [57]Fe, [59]Co, [60]Ni, [65]Cu, [66]Zn, [71]Ga, [85]Rb, [88]Sr, [89]Y, [90]Zr, [93]Nb, [115]In, [118]Sn, [119]Sn, [121]Sb, [123]Sb, [138]Ba, [178]Hf, [181]Ta, [184]W, [208]Pb, [232]Th, and [238]U. Data for Li, P, Rb, In, Sn, Sb and Pb are not presented because these elements were either too incompatible or too volatile under the experimental conditions. The laser was operated with a frequency of 10 to 15 Hz using a spot size that varied from 20 to 100 microns in diameter, depending on the
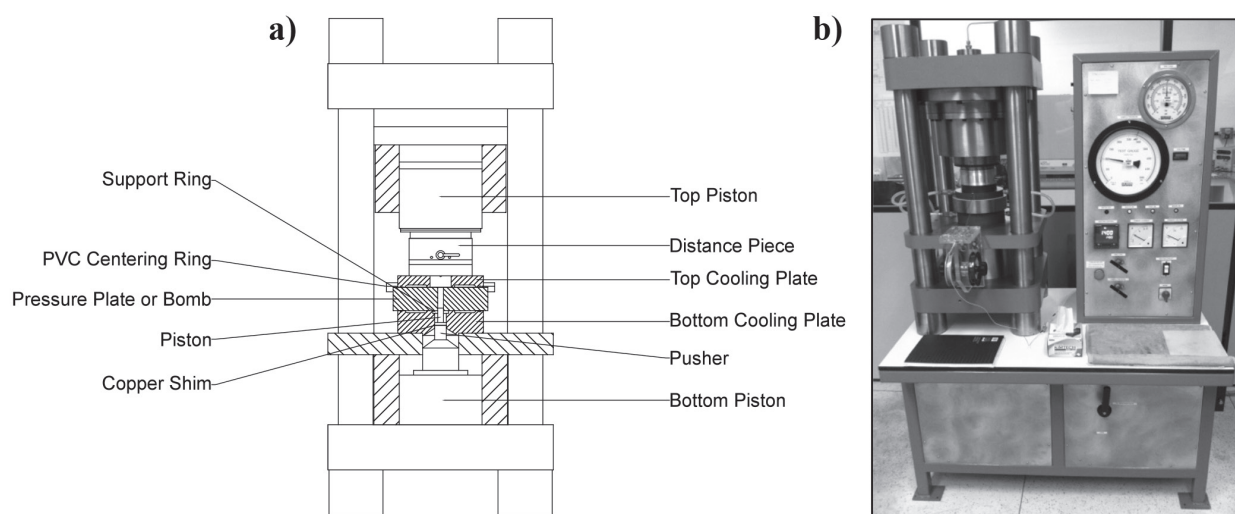
Figure 4 - Schematic drawing (a) and photograph of the Bristol-design end-loaded piston cylinder apparatus used in this study. Schematic drawing courtesy of Charles Clapham (University of Bristol).

size of the phase and whether melt inclusions were present. Count rates were normalized to either ^{29}Si (for silicate melts) or ^{47}Ti (for rutile) with concentrations defined by electron microprobe and stoichiometry, respectively. Normalized counts were then transformed into concentrations using the NIST-SRM 610 silicate glass as external reference standard assuming the concentrations given in Jochum et al. (2011). The standard NIST-SRM 612 silicate glass was used to monitor the variability and accuracy of measurements. For each phase, we collected between 5 and 15 individual spot analyses, with each spectrum consisting of 20 seconds of background measurements and 40 seconds of sample integration (Fig. 5). However, in many cases, due to the severity of cross-contamination between the rutile and silicate glass signal, either because of the small size of rutile crystals, presence of melt inclusions in rutile, or presence of micro-crystals of rutile in the silicate melt, several individual spot analyses had to be discarded (Fig. 5). To assess the level of contamination we monitored the signals of ^{29}Si, ^{23}Na, ^{138}Ba and ^{47}Ti, and only considered spectrum that showed no or very little signal cross-

contamination. For many samples we could not obtain "clean" uncontaminated analyses of either rutile and silicate melt, hence the gaps in the data presented in the paper.

RESULTS AND DISCUSSION

In total, our study resulted in 80 individual experimental samples, which produced upon quenching euhedral to subhedral rutile crystals of sizes ranging from about 1 to 500 microns and homogeneous silicate glass. No other phase was observed. Examples of typical run products are illustrated in Fig. 6. The major element composition of silicate glasses (only selected samples for which trace element contents in both rutile and silicate melt could be determined) is presented in Table III. The trace element composition of silicate glasses and rutile of selected samples is presented in Table IV, and rutile/silicate-melt partition coefficients, calculated by dividing the concentrations of trace elements, is given in Table V. Composition SM20 yielded the largest rutile crystals, hence we were able to analyze all experiments in the oxygen fugacity series. Composition SKHDRH1 yielded extremely small rutile crystals, which we were not able to analyze for
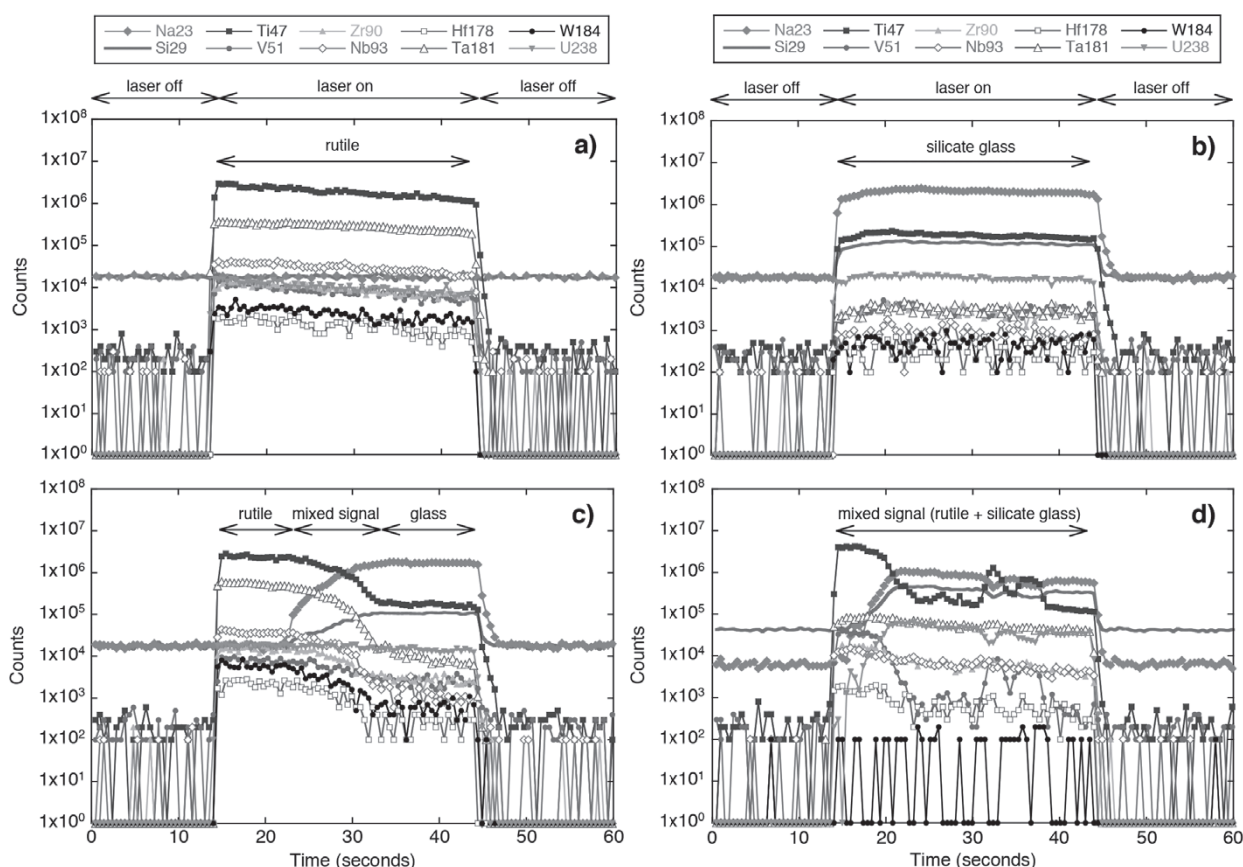
Figure 5 - Examples of laser time-resolved laser-ablation ICP-MS spectra recorded in this study. a) "Clean" rutile spectrum. b) "Clean" silicate glass spectrum. c) Mixed rutile (15-22 sec) and silicate glass (36-45 sec) spectrum. In this case, the laser drilled trough the rutile crystal and reached the silicate glass, resulting in a mixed signal from around seconds 22 to 36. d) Completely mixed signal between rutile and silicate melt where it is difficult to extract a "clean" rutile and/or silicate glass signal. This spectrum was not integrated.

trace elements and therefore have no data to present. Composition SKHDAN1 also yielded very small rutile crystals, but we were able to collect at least one "clean" rutile analysis in a few samples with this composition, which cover the various doping cocktails we used at oxygen fugacities ranging from reduced to intermediate to oxidized.

Calculated rutile/silicate-melt partitioning coefficients (Table V) are in good agreement with literature data. Specifically, our experiments with composition SM20 at 1300°C and log fO_2 of -3.4 (SP130813-3 and SP180213-5) resulted in partition coefficients that are consistent with those reported by Klemme et al. (2005) for their equivalent experiment RT10-20, attesting for attainment

of equilibrium. We note, however, that there is a systematic change in partitioning coefficients calculated for experiments with composition SM20 as a function of oxygen fugacity (Fig. 7). While this behavior is normally assumed to be due to changes in valence states, we observe that such changes occur even for trace-element cations which are known from previous studies to display a constant valence state (i.e. homovalent elements) over the range of oxygen fugacity conditions covered in our experiments (Fig. 7a). This change must therefore result from the effect of another variable, which we identified to be melt composition. There is a systematic change in melt major-element composition with oxygen fugacity, with noticeable
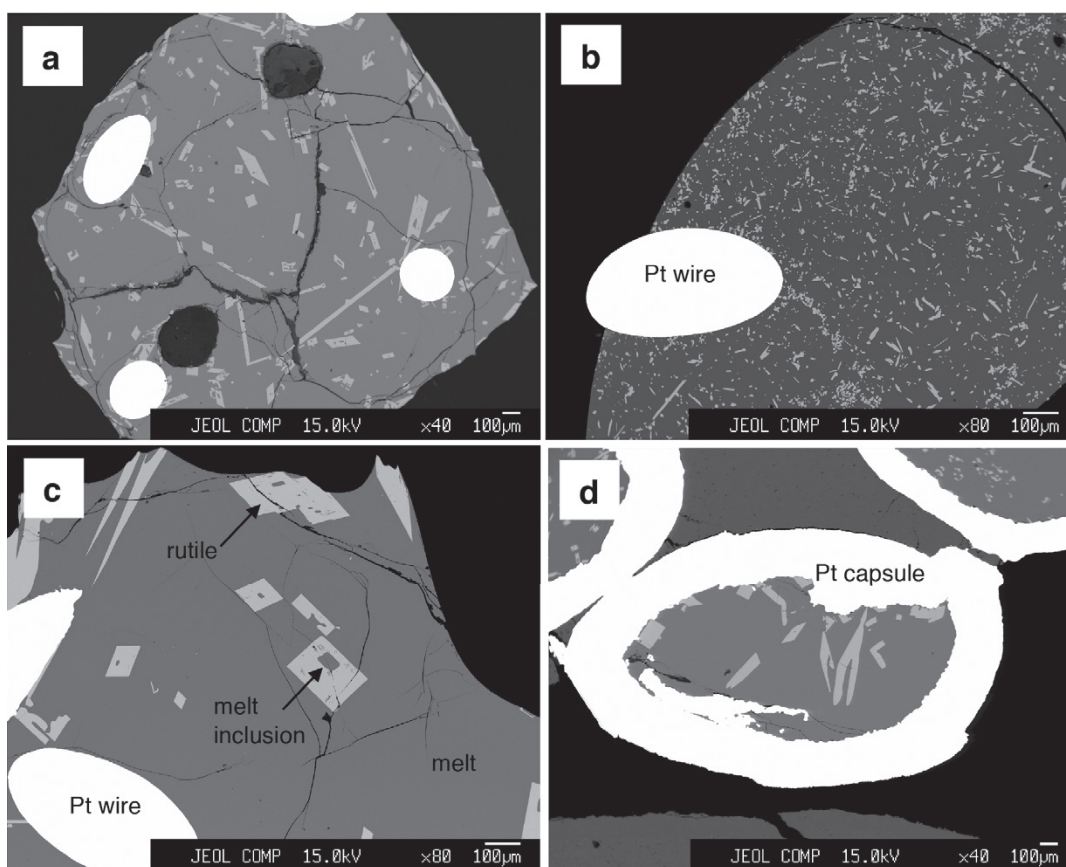
Figure 6 - Backscattered electron (BSE) images of representative experiments. a) Typical experimental product obtained for composition SM20 in 1-bar high-temperature experiments containing rutile crystals (light gray) and silicate melt quenched to glass (dark grey). White areas are Pt wire remnants. Dark surroundings are epoxy. b) Example of 1-bar high-temperature experimental product obtained with composition SKHDRH1. Rutile crystals produced with this composition were too small to be analyzed by laser-ablation ICP-MS. c) Detail showing rutile crystals containing melt inclusions. d) Example of experiment at high-pressure with PtO$_2$.

decrease in Ti and Na and increase in Si, Al, Ca and Mg with decreasing fO$_2$, which results in a gradual increase in melt polymerization from oxidized to reducing conditions as evidenced by melt descriptors such as optical basicity (Λ) and NBO/T (Table III, Fig. 8). The most likely explanation for this change is the progressive loss of Na by volatility with decreasing fO$_2$. Despite our efforts, we also noted that a significant proportion of Fe was lost to Pt wire in experiments at log fO$_2$ -7, -8 and -9 (Table III), hence these specific experiments with composition SM20 should be interpreted with caution.

PARTITIONING AND SPECIATION OF HETEROVALENT ELEMENTS

Klemme et al. (2005) reported rutile/silicate-melt partition coefficients for vanadium, noting that the lowest values were obtained for the most oxidizing experiments. However, they found no consistent trend with oxygen fugacity. Our results for composition SM20 show a systematic increase in V partition coefficients from ∼ 0.04 to ∼ 19 towards reducing conditions (Fig 7b). However, as noted previously, there is a systematic change in melt composition concomitant with the change in oxygen fugacity that most certainly affected the partitioning of all elements

TABLE III
Major element composition (in cg/g) of silicate melts (glass) determined by electron microprobe.

Run	log fO$_2$	SiO$_2$	TiO$_2$	Al$_2$O$_3$	Na$_2$O	K$_2$O	CaO	MgO	FeO	MnO	Total	n	Basicity*	NBO/T$^\$$
SP070713-4	-12.0	64.8 (0.8)	7.75 (0.13)	12.8 (0.15)	1.30 (0.08)	2.39 (0.06)	4.10 (0.09)	3.10 (0.06)	2.01 (0.13)	0.38 (0.07)	98.6	5	0.542	0.15
SP220713-4	-11.0	62.5 (0.2)	9.42 (0.13)	12.2 (0.18)	2.89 (0.07)	2.53 (0.04)	4.05 (0.12)	2.97 (0.04)	3.00 (0.14)	0.47 (0.05)	100.0	5	0.533	0.21
SP300713-3	-10.0	62.2 (0.8)	8.87 (0.17)	12.3 (0.21)	2.76 (0.07)	2.50 (0.04)	3.89 (0.06)	2.95 (0.06)	2.93 (0.18)	0.49 (0.07)	99.0	5	0.551	0.20
SP070813-2	-9.0	62.6 (0.9)	9.65 (0.21)	12.7 (0.15)	4.83 (0.11)	2.20 (0.06)	4.07 (0.15)	3.02 (0.09)	0.08 (0.03)	0.39 (0.03)	99.5	5	0.552	0.19
SP100813-5	-8.0	64.9 (0.2)	7.96 (0.17)	12.6 (0.05)	3.37 (0.16)	2.83 (0.05)	4.05 (0.08)	3.13 (0.24)	0.01 (0.01)	0.32 (0.05)	99.1	5	0.546	0.16
SP050313-3	-7.0	58.6 (0.4)	14.2 (0.30)	11.4 (0.18)	7.11 (0.20)	2.17 (0.03)	3.65 (0.12)	2.85 (0.15)	0.49 (0.06)	0.46 (0.13)	100.9	5	0.564	0.25
SP020313-5	-6.0	53.9 (0.4)	17.1 (0.29)	10.6 (0.14)	8.36 (0.22)	2.05 (0.05)	3.30 (0.04)	2.49 (0.04)	2.18 (0.11)	0.43 (0.04)	100.5	5	0.575	0.32
SP270213-5	-5.0	53.1 (0.4)	18.1 (0.42)	10.6 (0.06)	8.87 (0.28)	2.03 (0.04)	3.22 (0.04)	2.48 (0.10)	1.59 (0.10)	0.45 (0.05)	100.5	5	0.577	0.32
SP180213-5	-3.4	48.4 (0.2)	21.3 (0.61)	9.52 (0.09)	10.0 (0.22)	1.87 (0.06)	2.96 (0.09)	2.23 (0.19)	2.13 (0.16)	0.41 (0.07)	98.9	5	0.586	0.37
SP130813-3	-3.4	50.7 (0.2)	20.2 (0.16)	10.0 (0.12)	9.38 (0.15)	2.13 (0.07)	3.10 (0.05)	2.36 (0.06)	2.27 (0.07)	0.37 (0.09)	100.6	5	0.583	0.35
SP210213-5	-2.0	49.4 (0.2)	21.8 (0.22)	9.68 (0.04)	10.4 (0.20)	1.88 (0.02)	2.99 (0.07)	2.41 (0.12)	2.22 (0.12)	0.42 (0.07)	101.2	5	0.587	0.38
SP250713-4	-0.7	54.8 (0.3)	15.7 (0.15)	10.8 (0.12)	7.83 (0.22)	2.17 (0.06)	3.33 (0.06)	2.54 (0.08)	2.69 (0.07)	0.41 (0.07)	100.2	5	0.574	0.32
SP240213-5	0.0	49.0 (0.4)	21.5 (0.25)	9.57 (0.04)	10.0 (0.16)	2.00 (0.08)	2.96 (0.04)	2.26 (0.02)	2.13 (0.08)	0.33 (0.08)	99.8	5	0.586	0.36
PC100813	4.3	50.0 (0.3)	20.4 (0.32)	9.56 (0.09)	10.2 (0.17)	2.24 (0.02)	3.07 (0.02)	2.49 (0.01)	2.21 (0.01)	0.43 (0.02)	100.6	3	0.587	0.39

Values in parenthesis are standard deviation (1-sigma) of the mean of *n* measurements.

* Optical basicity calculated as described by Duffy (1993) assuming a value for TiO$_2$ of 0.61.

$^\$$ NBO/T calculated as described in Mills (1993).

TABLE III (continuation)

Run	log fO$_2$	SiO$_2$	TiO$_2$	Al$_2$O$_3$	Na$_2$O	K$_2$O	CaO	MgO	FeO	MnO	Total	n	Basicity*	NBO/T$
SP220713-1	-11.0	57.9 (0.2)	7.45 (0.12)	19.8 (0.24)	3.26 (0.08)	3.30 (0.06)	7.55 (0.14)	0.02 (0.01)	0.13 (0.02)	0.01 (0.02)	99.3	5	0.559	0.05
SP050313-1	-7.0	54.5 (0.3)	10.7 (0.34)	18.7 (0.06)	5.41 (0.63)	3.51 (0.05)	7.21 (0.11)	0.03 (0.05)	0.06 (0.02)	0.02 (0.02)	100.1	5	0.570	0.13
SP020313-1	-6.0	53.6 (0.4)	11.5 (0.31)	18.4 (0.08)	6.18 (0.04)	3.54 (0.08)	7.06 (0.13)	0.02 (0.01)	0.02 (0.01)	0.01 (0.02)	100.3	5	0.573	0.12
SP130813-2	-3.4	56.0 (0.6)	9.49 (0.28)	19.2 (0.21)	5.74 (0.17)	2.60 (0.04)	7.30 (0.09)	0.03 (0.01)	0.09 (0.06)	0.02 (0.02)	100.5	5	0.567	0.09
SP050313-4	-7.0	54.8 (0.2)	10.6 (0.16)	18.9 (0.20)	5.68 (0.09)	3.51 (0.04)	7.30 (0.16)	0.06 (0.06)	0.01 (0.01)	0.03 (0.02)	100.9	5	0.571	0.11
SP020313-2	-6.0	53.9 (0.5)	11.1 (0.37)	18.7 (0.14)	6.11 (0.18)	3.41 (0.05)	6.99 (0.11)	0.02 (0.02)	0.02 (0.02)	0.02 (0.03)	100.3	5	0.572	0.11
SP130813-1	-3.4	52.5 (0.5)	12.2 (0.18)	18.1 (0.16)	6.71 (0.15)	3.43 (0.04)	6.94 (0.12)	0.02 (0.01)	0.02 (0.04)	0.03 (0.02)	100.0	5	0.576	0.13
SP050313-2	-7.0	55.2 (0.3)	10.3 (0.05)	18.7 (0.06)	5.36 (0.07)	3.44 (0.07)	7.20 (0.11)	0.09 (0.09)	0.02 (0.02)	0.02 (0.02)	100.2	5	0.569	0.10
SP020313-3	-6.0	54.0 (0.1)	11.3 (0.26)	18.6 (0.07)	5.93 (0.24)	3.57 (0.13)	7.04 (0.07)	0.02 (0.02)	0.02 (0.03)	0.03 (0.04)	100.4	5	0.572	0.11
SP130813-4	-3.4	53.1 (0.2)	12.4 (0.40)	18.1 (0.08)	6.88 (0.17)	3.49 (0.06)	6.88 (0.08)	0.02 (0.01)	0.08 (0.04)	0.01 (0.02)	101.1	5	0.576	0.14

Values in parenthesis are standard deviation (1-sigma) of the mean of n measurements.

* Optical basicity calculated as described by Duffy (1993) assuming a value for TiO$_2$ of 0.61.

$ NBO/T calculated as described in Mills (1993).
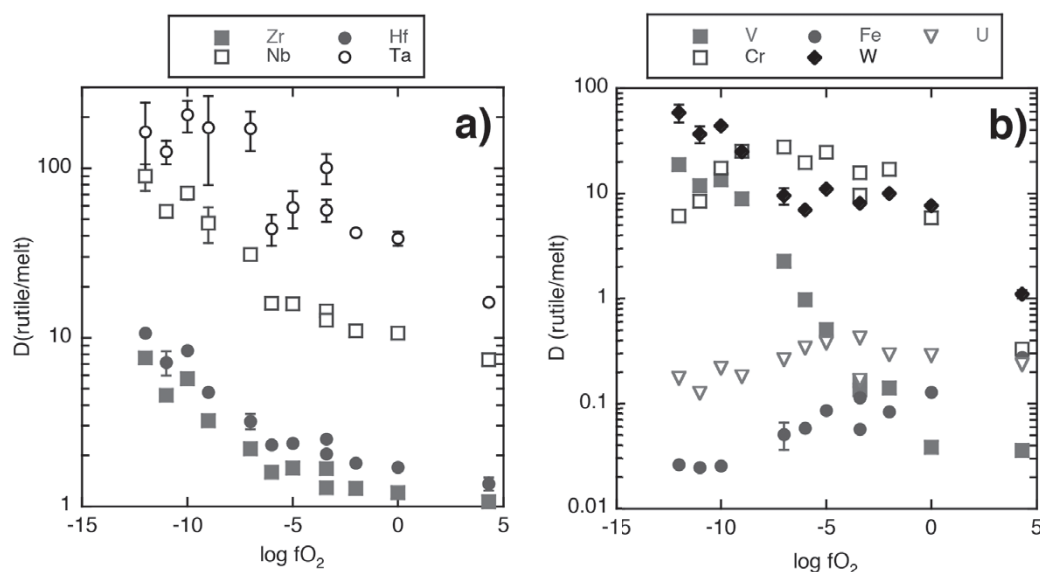
Figure 7 - Rutile/silicate-melt partition coefficient obtained for HFSEs (a) and several heterovalent elements (b) plotted against oxygen fugacity. Note that the systematic change in Zr, Hf, Nb and Ta partition coefficients with oxygen fugacity is in fact due to a concomitant change in melt composition (see Fig. 8) and not changes in valence states.
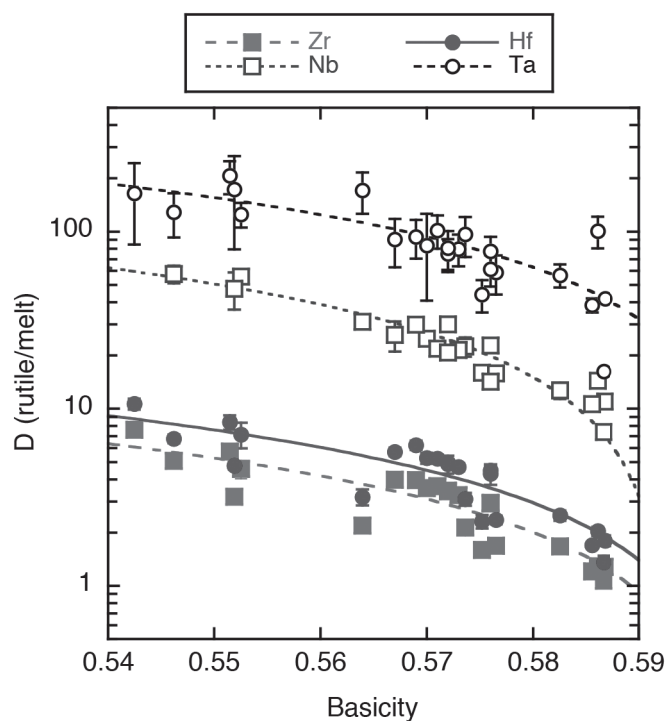

Figure 8 - Rutile/silicate-melt partition coefficient obtained for HFSEs plotted against the optical basicity of the silicate melt. See text for details on linear regressions.

TABLE IV
Trace element composition (in µg/g) of silicate melt (glass) and rutile determined by laser-ablation ICP-MS.

Silicate melt

Run	log fO$_2$	Na	Mg	Al	K	Ca	Sc	V	Cr	Mn	Fe	Co	Ni
SP070713-4 I	-12	10794 (324)	22199 (319)	92051 (1140)	26426 (1207)	36388 (421)	78.8 (3.3)	45.4 (1.0)	109.0 (2.1)	4332 (75)	17918 (168)	1.4 (0.0)	38.9 (0.8)
SP220713-4 I	-11	27675 (9)	24542 (462)	97907 (2144)	30631 (94)	38420 (2243)	97.8 (3.5)	71.5 (1.2)	97.5 (2.8)	6020 (110)	25734 (219)	31.9 (1.0)	67.0 (8.8)
SP300713-3z I	-10	21607 (197)	21642 (349)	89616 (1599)	26845 (176)	34090 (975)	103.2 (3.1)	61.1 (1.9)	47.6 (0.5)	5452 (83)	25640 (158)	34.7 (0.9)	30.6 (0.7)
SP070813-2 I	-9	43665 (905)	25387 (233)	103277 (3982)	26054 (559)	39566 (1414)	98.3 (3.1)	83.8 (5.0)	31.2 (5.4)	5293 (24)	548 (87)	0.7 (0.1)	0.7 (0.5)
SP100813-5 I	-8	28731 (371)	22776 (78)	92363 (514)	30701 (491)	35993 (291)	103.7 (1.4)	64.6 (1.5)	20.3 (1.8)	3235 (65)	215 (12)	0.4 (0.1)	0.4 (0.3)
SP050313-3 I	-7	83687 (599)	28527 (229)	109081 (1965)	32635 (319)	41270 (645)	109.3 (1.7)	215.3 (4.4)	38.0 (0.9)	6817 (76)	6821 (212)	9.9 (0.5)	9.8 (1.4)
SP020313-5 I	-6	113495 (1424)	29220 (671)	120754 (2317)	34385 (349)	47222 (1279)	124.3 (5.1)	311.7 (3.9)	54.7 (7.1)	7344 (125)	26455 (1040)	73.9 (2.1)	73.1 (7.5)
SP270213-5 I	-5	123570 (1631)	29589 (309)	118722 (1091)	35633 (322)	44276 (872)	118.8 (3.4)	341.7 (5.7)	41.2 (1.6)	7590 (7)	20282 (378)	44.2 (0.6)	55.3 (3.4)
SP130813-3 I	-3.4	145928 (593)	30776 (126)	129144 (1961)	42200 (643)	48533 (2396)	137.0 (3.1)	376.5 (6.4)	16.6 (2.6)	7761 (47)	32406 (477)	89.2 (2.1)	64.7 (3.6)
SP180213-5 I	-3.4	161021 (3338)	31311 (204)	131767 (2355)	37370 (390)	47635 (1399)	136.3 (0.9)	414.8 (1.3)	175.0 (31)	8038 (104)	37106 (582)	108.8 (2.4)	161.7 (4.0)
SP210213-5 I	-2	157975 (795)	30787 (135)	130998 (1041)	36785 (144)	46582 (464)	139.9 (1.0)	407.8 (1.5)	93.4 (3.4)	7876 (31)	34978 (179)	96.4 (0.8)	81.9 (1.6)
SP250713-4 I	-0.7	100577 (2477)	27498 (206)	114880 (1220)	34192 (446)	43938 (105)	123.9 (0.7)	277.4 (13)	1.3 (0.1)	6380 (63)	31921 (135)	103.4 (1.0)	242.0 (4.5)
SP240213-5 I	0	168890 (572)	32284 (251)	134881 (395)	42061 (539)	49187 (3011)	140.8 (2.5)	441.2 (9.3)	148.2 (0.6)	7485 (46)	35683 (267)	110.6 (1.2)	184.2 (13)
PC100813 I	4.3	192625 (1647)	31769 (382)	128167 (1813)	37763 (274)	51478 (1060)	137.6 (3.6)	448.6 (5.8)	374.6 (8.4)	6789 (105)	26409 (342)	116.5 (1.6)	161.9 (3.0)
SP220713-1 II	-11	85078 (1095)	236 (14)	167353 (2673)	56056 (1068)	105909 (3616)	29.7 (3.9)	10.9 (2.1)	3.5 (2.5)	13.3 (17)	326 (245)	bdl (--)	13.1 (2.4)
SP050313-1 II	-7	71039 (765)	279 (5)	221285 (3337)	60662 (762)	98870 (2212)	22.7 (1.2)	7.3 (0.6)	7.9 (0.6)	9.0 (0.8)	308 (20)	bdl (--)	32.2 (4.1)
SP020313-1 II	-6	83345 (808)	273 (11)	198066 (806)	60576 (547)	89840 (2554)	16.0 (1.2)	9.5 (0.5)	5.3 (1.6)	8.6 (3.4)	bdl (--)	bdl (--)	bdl (--)
SP130813-2 II	-3.4	76597 (1246)	286 (4)	200261 (2689)	42321 (629)	93280 (3199)	15.1 (2.6)	27.1 (0.9)	6.1 (1.3)	11.7 (2.5)	1002 (67)	bdl (--)	23.0 (3.2)
SP050313-4 III	-7	71383 (234)	275 (7)	216075 (3108)	60074 (342)	99094 (1276)	21.9 (1.8)	102.8 (2.0)	7.0 (0.8)	9.5 (1.1)	74 (20)	bdl (--)	5.7 (2.1)
SP020313-2 III	-6	78678 (419)	254 (12)	198025 (518)	57972 (545)	91391 (2408)	11.1 (2.8)	122.6 (4.6)	7.4 (0.9)	8.9 (3.1)	255 (160)	bdl (--)	5.3 (1.5)
SP130813-1 III	-3.4	96523 (102)	262 (8)	204063 (2761)	60027 (177)	87908 (3153)	16.7 (0.6)	159.4 (3.1)	6.1 (0.5)	13.1 (4.1)	770 (155)	bdl (--)	18.5 (4.5)
SP050313-2 IV	-7	66997 (610)	287 (4)	208356 (3672)	58362 (563)	92885 (1701)	89.1 (1.8)	115.8 (2.8)	32.7 (3.5)	11.5 (0.3)	99 (33)	2.2 (0.4)	5.7 (0.2)
SP020313-3 IV	-6	79398 (896)	294 (13)	197054 (2239)	60078 (343)	91385 (2852)	88.2 (3.8)	141.9 (4.6)	30.9 (3.0)	7.5 (0.7)	330 (88)	7.5 (1.6)	11.3 (2.3)
SP130813-4 IV	-3.4	94941 (423)	256 (2)	199393 (1962)	60249 (411)	92429 (5259)	82.2 (3.0)	197.5 (4.0)	15.7 (1.4)	10.3 (2.5)	1272 (123)	55.7 (3.1)	54.0 (5.9)

Compositions: I = SM-20, II = SKHANDl-a, III = SKHANDl-b, IV = SKHANDl-c. Values in parenthesis are standard deviation (1-sigma) of the mean of *n* measurements. bdl = below detection limit.

TABLE IV (continuation)

Rutile

Run		log fO$_2$	Na	Mg	Al	K	Ca	Sc	V	Cr	Mn	Fe	Co	Ni
SP070713-4	I	-12	7 (10)	251 (17)	5508 (211)	7 (7)	bdl (---)	71.4 (31)	850 (31)	666 (30)	17 (8)	472 (71)	0.7 (0.2)	13.3 (4.1)
SP220713-4	I	-11	28 (22)	236 (20)	2997 (55)	7 (2)	22 (38)	40.1 (3.6)	848 (51)	823 (27)	16 (3)	637 (32)	1.2 (0.5)	15.8 (5.0)
SP300713-3	I	-10	18 (7)	207 (18)	2978 (80)	32 (27)	1410 (1626)	60.3 (4.8)	822 (23)	830 (24)	19 (5)	658 (73)	1.7 (1.3)	7.3 (2.8)
SP070813-2	I	-9	21 (22)	237 (14)	1721 (69)	10 (14)	109 (162)	43.6 (1.6)	746 (33)	783 (19)	13 (1)	41 (18)	0.4 (0.1)	0.5 (0.3)
SP100813-5	I	-8	445 (---)	518 (---)	3349 (---)	291 (---)	bdl (---)	63.5 (---)	656 (---)	937 (---)	46 (---)	bdl (---)	0.7 (---)	bdl (---)
SP050313-3	I	-7	52 (24)	198 (5)	975 (15)	23 (6)	bdl (---)	30.4 (1.5)	488 (15)	1045 (71)	21 (4)	349 (101)	bdl (0.3)	1.5 (2.7)
SP020313-5	I	-6	19 (20)	163 (8)	865 (42)	11 (14)	1163 (1658)	26.6 (2.2)	303 (4)	1071 (15)	19 (2)	1555 (131)	1.2 (1.0)	8.2 (7.2)
SP270213-5	I	-5	89 (44)	217 (45)	865 (46)	26 (16)	1057 (502)	25.4 (2.0)	174 (5)	1011 (25)	32 (4)	1750 (34)	0.2 (0.1)	4.7 (2.5)
SP130813-3	I	-3.4	1 (---)	152 (---)	743 (---)	14 (---)	1060 (---)	29.2 (---)	62.5 (---)	260 (---)	49 (---)	3701 (---)	bdl (---)	8.8 (---)
SP180213-5	I	-3.4	9 (7)	96 (10)	603 (42)	bdl (---)	167 (107)	22.6 (1.4)	56.3 (3.7)	1680 (119)	34 (4)	2121 (139)	1.1 (0.2)	11.7 (0.6)
SP210213-5	I	-2	42 (38)	161 (7)	821 (11)	7 (0)	815 (---)	27.6 (3.1)	57.7 (2.5)	1586 (69)	54 (11)	2939 (215)	1.4 (0.4)	8.4 (5.0)
SP250713-4	I	-0.7	38 (44)	184 (27)	1040 (134)	15 (13)	1667 (---)	34.2 (1.4)	29.3 (0.7)	2.7 (0.2)	223 (16)	5671 (688)	2.4 (1.1)	31.4 (6.3)
SP240213-5	I	0	15 (10)	157 (6)	854 (11)	bdl (---)	1146 (762)	23.4 (1.4)	17.0 (1.1)	867 (111)	291 (4)	4593 (177)	1.0 (0.7)	16.0 (1.8)
PC100813	I	4.3	8 (4)	492 (75)	1656 (75)	bdl (---)	bdl (---)	29.9 (0.3)	16.1 (1.4)	123 (6)	4534 (284)	7300 (461)	4.0 (0.2)	11.0 (0.1)
SP220713-1	II	-11	178 (---)	60 (---)	7582 (---)	265 (---)	2984 (---)	2.58 (---)	29.4 (---)	177 (---)	2.3 (---)	bdl (---)	bdl (---)	15.7 (---)
SP050313-1	II	-7	331 (---)	72 (---)	3178 (---)	64 (---)	4130 (---)	0.64 (---)	21.9 (---)	312 (---)	bdl (---)	145 (---)	bdl (---)	bdl (---)
SP020313-1	II	-6	362 (---)	62 (---)	3788 (---)	306 (---)	2408 (---)	1.22 (---)	18.5 (---)	331 (---)	bdl (---)	237 (---)	bdl (---)	bdl (---)
SP130813-2	II	-3.4	242 (---)	49 (---)	3778 (---)	107 (---)	4085 (---)	1.74 (---)	18.4 (---)	317 (---)	bdl (---)	769 (---)	bdl (---)	2.2 (---)
SP050313-4	III	-7	687 (---)	59 (---)	5489 (---)	574 (---)	1895 (---)	0.92 (---)	366 (---)	371 (---)	bdl (---)	bdl (---)	0.7 (---)	bdl (---)
SP020313-2	III	-6	75 (---)	58 (---)	3313 (---)	58 (---)	bdl (---)	2.22 (---)	266 (---)	428 (---)	bdl (---)	bdl (---)	0.7 (---)	bdl (---)
SP130813-1	III	-3.4	15 (---)	64 (---)	3622 (---)	25 (---)	bdl (---)	1.47 (---)	62.7 (---)	362 (---)	bdl (---)	664 (---)	0.5 (---)	bdl (---)
SP050313-2	IV	-7	1276 (---)	70 (---)	6502 (---)	1103 (---)	4338 (---)	46.5 (---)	377 (---)	1314 (---)	bdl (---)	bdl (---)	bdl (---)	1.2 (---)
SP020313-3	IV	-6	84 (---)	65 (---)	2930 (---)	49 (---)	1299 (---)	40.0 (---)	256 (---)	1541 (---)	bdl (---)	152 (---)	bdl (---)	bdl (---)
SP130813-4	IV	-3.4	bdl (---)	56 (---)	2329 (---)	bdl (---)	bdl (---)	39.3 (---)	67.6 (---)	736 (---)	bdl (---)	367 (---)	1.3 (---)	4.4 (---)

Compositions: I = SM-20, II = SKHAND1-a, III = SKHAND1-b, IV = SKHAND1-c. Values in parenthesis are standard deviation (1-sigma) of the mean of *n* measurements. bdl = below detection limit.

TABLE IV (continuation)

Silicate melt

Run	log fO$_2$	Na	Mg	Al	K	Ca	Sc	V	Cr	Mn	Fe	Co	Ni	U	n
SP070713-4 I	-12	8.2 (2.7)	3.5 (0.4)	0.6 (0.2)	451 (6)	97.3 (6.9)	59.4 (3.0)	4.6 (0.6)	193 (1)	1.63 (0.09)	1.62 (0.59)	0.97 (0.12)	29.3 (1.6)	77.6 (2.7)	3
SP220713-4 I	-11	8.6 (2.6)	5.1 (1.2)	1.8 (0.4)	482 (12)	106.3(4.6)	77.8 (5.4)	7.2 (0.5)	210 (3)	2.15 (0.31)	2.02 (0.24)	2.84 (0.22)	31.5 (0.6)	74.4 (1.2)	3
SP300713-3 I	-10	4.6 (1.2)	2.3 (0.4)	4.2 (0.4)	429 (8)	89.4 (1.0)	69.6 (1.7)	5.1 (0.3)	184 (3)	2.20 (0.15)	1.21 (0.11)	2.57 (0.07)	27.0 (0.4)	57.5 (1.2)	3
SP070813-2 I	-9	8.4 (1.1)	4.0 (0.5)	7.9 (0.9)	510 (15)	115.9(7.0)	98.4 (2.1)	8.8 (1.6)	209 (3)	2.81 (0.10)	2.55 (0.52)	3.62 (0.33)	33.0 (1.8)	87.9 (1.3)	3
SP100813-5 I	-8	5.7 (0.8)	3.5 (0.3)	7.5 (0.7)	462 (6)	105.1(1.4)	79.0 (1.2)	5.6 (0.6)	210 (1)	2.20 (0.06)	0.85 (0.17)	13.83(1.00)	32.6 (0.8)	147.1(2.7)	3
SP050313-3 I	-7	16.9 (0.5)	9.4 (0.7)	64.8 (1.4)	509 (9)	109.6(1.5)	124.4 (1.0)	16.4 (0.9)	221 (3)	3.84 (0.22)	3.98 (0.64)	4.15 (0.50)	31.8 (0.3)	80.3 (0.7)	5
SP020313-5 I	-6	23.7 (4.5)	10.5 (1.5)	96.7 (1.0)	590 (19)	133.5(4.1)	166.1 (4.4)	30.3 (1.3)	252 (4)	5.08 (0.42)	7.93 (1.30)	2.89 (0.19)	38.7 (1.5)	86.5 (1.6)	3
SP270213-5 I	-5	30.9 (1.8)	10.7 (0.9)	98.0 (3.2)	561 (8)	125.7(1.4)	169.1 (3.0)	36.1 (1.2)	241 (3)	5.30 (0.27)	12.27(0.79)	1.37 (0.10)	36.4 (0.7)	78.5 (1.9)	3
SP130813-3 I	-3.4	44.1 (4.7)	17.8 (2.0)	127.6(3.0)	625 (5)	139.2(2.2)	195.8 (6.1)	48.4 (1.9)	261 (2)	6.14 (0.20)	13.62(0.34)	bdl (---)	40.3 (0.6)	264.2(1.0)	4
SP180213-5 I	-3.4	95.4 (6.1)	15.1 (1.3)	106.2(5.4)	610 (11)	136.1(3.9)	206.9 (3.8)	62.9 (6.0)	258 (3)	6.67 (0.17)	23.72(2.74)	6.37 (0.68)	39.4 (0.9)	106.3(2.4)	3
SP210213-5 I	-2	61.7 (0.7)	14.0 (1.2)	104.4(2.2)	596 (5)	132.9(1.4)	199.4 (1.0)	60.2 (1.0)	256 (1)	6.44 (0.19)	22.97(0.42)	2.99 (0.31)	37.6 (0.2)	85.2 (1.0)	3
SP250713-4 I	-0.7	88.1 (5.8)	13.3 (1.8)	112.4(6.3)	550 (8)	118.0(1.2)	148.2 (1.8)	25.7 (2.6)	230 (1)	4.43 (0.10)	9.14 (1.16)	3.66 (0.24)	34.5 (0.5)	51.0 (1.0)	3
SP240213-5 I	0	229 (19)	17.3 (3.9)	108.6(2.4)	654 (2)	143.8(2.6)	217.3 (3.4)	63.4 (2.9)	275 (3)	7.14 (0.12)	29.84(0.46)	4.06 (0.25)	42.5 (1.1)	81.7 (1.7)	3
PC100813 I	4.3	295 (6)	159 (2.4)	101.1(1.2)	667 (14)	150.7(4.5)	216.5 (6.1)	77.8 (2.2)	278 (7)	7.33 (0.25)	40.22(1.68)	139 (3.7)	44.3 (1.2)	99.8 (1.8)	5
SP220713-1 II	-11	18.1 (4.7)	7.9 (1.6)	18.0 (6.5)	224 (8)	13.6 (2.1)	264.0 (11)	189 (8)	30.8 (2.2)	335 (14)	54.05(0.99)	3.94 (1.05)	1.17 (0.34)	10.9 (0.7)	3
SP050313-1 II	-7	15.8 (0.7)	8.2 (0.4)	22.4 (0.7)	259 (2)	15.2 (0.4)	301.3 (6.1)	165 (8)	35.4 (0.6)	307 (16)	52.65 (24.7)	6.44 (1.04)	1.56 (0.07)	6.3 (0.8)	5
SP020313-1 II	-6	12.9 (1.4)	5.6 (0.6)	17.8 (3.9)	247 (4)	15.5 (0.8)	294.9 (7.8)	209 (5)	34.7 (1.2)	350 (6)	47.23 (1.88)	4.22 (1.10)	1.31 (0.10)	8.4 (0.4)	4
SP130813-2 II	-3.4	22.8 (6.8)	4.5 (0.7)	137.5 (11)	254 (7)	15.5 (0.5)	359.3 (9.0)	131 (24)	35.2 (0.4)	252 (6)	22.69 (5.26)	25.47(2.49)	1.58 (0.06)	103.9(1.4)	4
SP050313-4 III	-7	14.7 (1.5)	7.7 (0.9)	17.6 (1.3)	265 (5)	15.6 (0.3)	485.4 (3.1)	280 (3)	35.8 (0.4)	403 (4)	63.26 (4.92)	6.73 (0.87)	1.61 (0.06)	5.6 (1.1)	5
SP020313-2 III	-6	7.1 (4.7)	5.1 (2.1)	25.5 (4.5)	249 (5)	15.6 (0.6)	501.8 (8.8)	282 (6)	35.0 (1.1)	435 (7)	63.18 (4.15)	3.77 (0.68)	2.24 (0.11)	10.5 (0.3)	4
SP130813-1 III	-3.4	21.6 (3.8)	8.6 (2.2)	43.6 (3.9)	254 (4)	16.2 (0.4)	586.4 (5.2)	526 (8)	35.9 (1.9)	481 (6)	113.70(3.49)	12.59(0.84)	1.59 (0.09)	105.6(4.0)	4
SP050313-2 IV	-7	13.9 (1.4)	7.8 (0.8)	39.1 (1.2)	310 (3)	75.2 (1.1)	89.3 (2.7)	17.1 (1.2)	126 (1)	2.65 (0.09)	9.02 (1.31)	8.15 (0.57)	24.9 (0.3)	56.4 (1.0)	5
SP020313-3 IV	-6	10.4 (2.6)	2.5 (0.7)	69.6 (4.9)	311 (7)	86.3 (3.4)	101.8 (2.6)	18.9 (1.4)	127 (3)	3.12 (0.32)	13.25(1.91)	6.83 (1.89)	27.3 (0.5)	51.6 (2.7)	5
SP130813-4 IV	-3.4	23.2 (3.9)	6.0 (1.2)	93.8 (4.2)	317 (5)	87.0 (1.8)	111.4 (2.7)	26.3 (1.5)	126 (2)	3.44 (0.41)	11.84(0.76)	19.45(1.12)	27.7 (0.5)	111.3(4.6)	5

Compositions: I = SM-20, II = SKHAND1-a, III = SKHAND1-b, IV = SKHAND1-c. Values in parenthesis are standard deviation (1-sigma) of the mean of *n* measurements. bdl = below detection limit.

TABLE IV (continuation)

Rutile

Run	log fO$_2$	Na	Mg	Al	K	Ca	Sc	V	Cr	Mn	Fe	Co	Ni	U	n
SP070713-4 I	-12	105 (1)	71 (8)	bdl (--)	0.30 (0.27)	0.55 (0.13)	452 (25)	412 (48)	0.10 (0.12)	17.3 (0.7)	265 (84)	57.0 (8.4)	0.077 (0.049)	13.5 (0.2)	3
SP220713-4 I	-11	118 (8)	69 (5)	bdl (--)	0.61 (0.61)	0.18 (0.05)	356 (34)	401 (7)	0.12 (0.18)	15.4 (1.2)	254 (27)	103.7 (17)	0.048 (0.043)	9.3 (0.2)	3
SP300713-3 I	-10	69 (5)	36 (4)	bdl (--)	0.38 (0.33)	0.19 (0.14)	399 (22)	366 (20)	0.15 (0.15)	18.5 (1.2)	250 (47)	112.2 (9.1)	0.018 (0.003)	12.5 (0.9)	3
SP070813-2 I	-9	90 (4)	57 (2)	bdl (--)	0.23 (0.22)	0.19 (0.07)	314 (15)	416 (64)	0.02 (0.04)	13.4 (0.4)	442 (222)	90.1 (8.1)	0.020 (0.009)	15.9 (2.7)	5
SP100813-5 I	-8	83 (--)	48 (--)	bdl (--)	4.71 (--)	1.57 (--)	401 (--)	324 (--)	2.53 (--)	14.9 (--)	110 (--)	193.0 (--)	0.383 (0.191)	42.0 (--)	1
SP050313-3 I	-7	59 (7)	34 (4)	2.83 (1.42)	0.32 (0.05)	0.11 (0.14)	272 (19)	507 (11)	0.10 (0.04)	12.2 (1.0)	682 (143)	39.5 (5.1)	0.016 (0.008)	21.0 (0.5)	3
SP020313-5 I	-6	77 (9)	47 (3)	1.47 (0.88)	0.33 (0.35)	0.11 (0.02)	265 (11)	484 (6)	0.02 (0.05)	11.7 (0.3)	349 (44)	20.1 (1.6)	0.025 (0.035)	29.2 (2.6)	4
SP270213-5 I	-5	105 (5)	65 (3)	1.49 (0.43)	0.44 (0.18)	0.22 (0.11)	285 (5)	573 (17)	0.14 (0.09)	12.5 (0.3)	721 (171)	15.1 (1.4)	0.029 (0.013)	29.6 (2.7)	5
SP130813-3 I	-3.4	82 (--)	50 (--)	0.33 (--)	0.12 (--)	0.13 (--)	253 (--)	696 (--)	0.01 (--)	12.5 (--)	1375 (--)	16.6 (--)	0.027 (0.014)	44.0 (--)	1
SP180213-5 I	-3.4	77 (9)	136 (68)	1.38 (1.04)	0.15 (0.07)	0.20 (0.16)	345 (16)	800 (42)	0.06 (0.07)	16.7 (1.0)	1348 (127)	51.3 (1.6)	0.037 (0.028)	44.6 (4.6)	6
SP210213-5 I	-2	74 (11)	49 (6)	1.58 (0.25)	0.24 (0.11)	0.28 (0.02)	256 (13)	662 (20)	0.06 (0.05)	11.6 (0.7)	960 (21)	29.9 (2.3)	0.042 (0.019)	25.0 (0.7)	3
SP250713-4 I	-0.7	76 (2)	52 (13)	2.62 (0.45)	0.51 (0.38)	0.26 (0.10)	317 (33)	578 (41)	0.19 (0.21)	13.7 (1.1)	882 (196)	63.3 (3.5)	0.039 (0.032)	48.2 (1.5)	4
SP240213-5 I	0	55 (4)	34 (4)	1.25 (0.78)	0.16 (0.15)	0.11 (0.05)	262 (5)	675 (13)	0.02 (0.03)	12.1 (0.3)	1149 (105)	31.0 (1.3)	0.011 (0.008)	23.4 (0.9)	6
PC100813 I	4.3	37 (1)	19 (5)	2.57 (0.82)	1.03 (0.12)	0.18 (0.02)	232 (1)	576 (6)	bdl (--)	9.9 (0.9)	653 (6)	154.0 (4.5)	0.003 (0.003)	23.4 (1.0)	2
SP220713-1 II	-11	151 (--)	90 (--)	bdl (--)	2.76 (--)	0.41 (--)	1154 (--)	3694 (--)	0.36 (--)	1699 (--)	2060 (--)	15.7 (--)	0.100 (--)	0.3 (--)	1
SP050313-1 II	-7	79 (--)	64 (--)	bdl (--)	0.21 (--)	0.08 (--)	1072 (--)	4102 (--)	0.09 (--)	1622 (--)	4402 (--)	20.1 (--)	0.175 (--)	1.4 (--)	1
SP020313-1 II	-6	80 (--)	64 (--)	bdl (--)	2.24 (--)	bdl (--)	959 (--)	4478 (--)	0.12 (--)	1640 (--)	3771 (--)	12.7 (--)	0.076 (--)	2.5 (--)	1
SP130813-2 II	-3.4	88 (--)	66 (--)	2.13 (--)	0.09 (--)	0.27 (--)	1427 (--)	3424 (--)	0.14 (--)	1442 (--)	2053 (--)	43.1 (--)	0.016 (--)	113.9 (--)	1
SP050313-4 III	-7	99 (--)	56 (--)	0.06 (--)	3.54 (--)	0.40 (--)	1774 (--)	6086 (--)	0.91 (--)	2103 (--)	6447 (--)	15.6 (--)	0.092 (--)	1.4 (--)	1
SP020313-2 III	-6	104 (--)	48 (--)	0.27 (--)	0.15 (--)	bdl (--)	1717 (--)	5859 (--)	0.18 (--)	2151 (--)	4729 (--)	14.3 (--)	0.068 (--)	2.8 (--)	1
SP130813-1 III	-3.4	103 (--)	67 (--)	4.62 (--)	bdl (--)	0.25 (--)	1715 (--)	7474 (--)	bdl (--)	2156 (--)	6982 (--)	10.1 (--)	0.072 (--)	27.8 (--)	1
SP050313-2 IV	-7	83 (--)	53 (--)	3.38 (--)	5.02 (--)	1.64 (--)	354 (--)	509 (--)	2.59 (--)	16.5 (--)	842 (--)	76.4 (--)	0.471 (--)	32.6 (--)	1
SP020313-3 IV	-6	77 (--)	55 (--)	6.44 (--)	0.42 (--)	0.31 (--)	351 (--)	566 (--)	0.11 (--)	15.2 (--)	1073 (--)	67.4 (--)	0.116 (--)	32.7 (--)	1
SP130813-4 IV	-3.4	94 (--)	61 (--)	8.38 (--)	0.23 (--)	0.14 (--)	329 (--)	600 (--)	bdl (--)	14.8 (--)	915 (--)	59.3 (--)	bdl (--)	76.8 (--)	1

Compositions: I = SM-20, II = SKHAND1-a, III = SKHAND1-b, IV = SKHAND1-c. Values in parenthesis are standard deviation (1-sigma) of the mean of *n* measurements. bdl = below detection limit.

TABLE V

Rutile/silicate melt partition coefficients.

Run	log fO$_2$	D(Na)	D(Mg)	D(Al)	D(K)	D(Ca)	D(Sc)	D(V)	D(Cr)	D(Mn)	D(Fe)	D(Co)	D(Ni)
SP070713-4 I	-12	<7e-4(--)	0.0113(0.0008)	0.0598(0.0024)	<3e-4(--)	-- (--)	0.907(0.391)	18.72(0.81)	6.1(0.3)	0.0039(0.0018)	0.026(0.004)	0.498(0.141)	0.34(0.11)
SP220713-4 I	-11	<1e-3(--)	0.0096(0.0008)	0.0306(0.0009)	<2e-4(--)	<6e-4(--)	0.410(0.040)	11.85(0.74)	8.4(0.4)	0.0026(0.0004)	0.025(0.001)	0.038(0.015)	0.24(0.08)
SP300713-3 I	-10	<8e-4(--)	0.0096(0.0008)	0.0332(0.0011)	<1e-3(--)	<4e-2(--)	0.585(0.050)	13.45(0.56)	17.4(0.5)	0.0035(0.0010)	0.026(0.003)	0.049(0.037)	0.24(0.09)
SP070813-2 I	-9	<5e-4(--)	0.0093(0.0006)	0.0167(0.0009)	<4e-4(--)	<3e-3(--)	0.444(0.021)	8.90(0.66)	25.1(4.4)	0.0024(0.0002)	0.074(0.035)	0.596(0.190)	0.76(0.76)
SP100813-5 I	-8	<1e-2(--)	0.0227(0.0018)	0.0363(0.0015)	<9e-3(--)	-- (--)	0.612(0.044)	10.15(0.47)	46.1(4.7)	0.0142(0.0019)	-- (--)	1.903(0.790)	-- (--)
SP050313-3 I	-7	<6e-4(--)	0.0069(0.0002)	0.0089(0.0002)	<7e-4(--)	-- (--)	0.278(0.014)	2.265(0.084)	27.5(2.0)	0.0031(0.0006)	0.051(0.015)	-- (--)	0.15(0.27)
SP020313-5 I	-6	<2e-4(--)	0.0056(0.0003)	0.0072(0.0004)	<3e-4(--)	<2e-2(--)	0.214(0.020)	0.971(0.017)	19.6(2.6)	0.0026(0.0003)	0.059(0.005)	0.016(0.014)	0.11(0.10)
SP270213-5 I	-5	<7e-4(--)	0.0073(0.0015)	0.0073(0.0004)	<7e-4(--)	<2e-2(--)	0.214(0.018)	0.508(0.016)	24.6(1.2)	0.0042(0.0005)	0.086(0.002)	0.005(0.001)	0.09(0.05)
SP130813-3 I	-3.4	<1e-5(--)	0.0049(0.0004)	0.0058(0.0002)	<3e-4(--)	<2e-2(--)	0.213(0.016)	0.166(0.007)	15.7(2.6)	0.0063(0.0008)	0.114(0.012)	-- (--)	0.14(0.05)
SP180213-5 I	-3.4	<1e-4(--)	0.0031(0.0003)	0.0046(0.0003)	-- (--)	<3e-3(--)	0.166(0.010)	0.136(0.009)	9.6(1.8)	0.0042(0.0005)	0.057(0.004)	0.010(0.002)	0.07(0.00)
SP210213-5 I	-2	<3e-4(--)	0.0052(0.0002)	0.0063(0.0001)	<2e-4(--)	<1e-2(--)	0.197(0.022)	0.142(0.006)	17.0(1.0)	0.0069(0.0014)	0.084(0.006)	0.015(0.004)	0.10(0.06)
SP250713-4 I	-0.7	<4e-4(--)	0.0067(0.0010)	0.0091(0.0012)	<5e-4(--)	<3e-2(--)	0.276(0.011)	0.106(0.005)	2.1(0.3)	0.0350(0.0026)	0.178(0.022)	0.023(0.011)	0.13(0.03)
SP240213-5 I	0	<1e-4(--)	0.0049(0.0002)	0.0063(0.0001)	-- (--)	<2e-2(--)	0.166(0.010)	0.039(0.003)	5.9(0.7)	0.0389(0.0006)	0.129(0.005)	0.009(0.006)	0.09(0.01)
PC100813 I	4.3	<5e-5(--)	0.0155(0.0003)	0.0129(0.0006)	-- (--)	-- (--)	0.217(0.006)	0.036(0.003)	0.33(0.02)	0.6678(0.0431)	0.276(0.018)	0.034(0.002)	0.07(0.00)
SP220713-1 II	-11	<2e-3(--)	0.2566(0.0256)	0.0453(0.0020)	<4e-3(--)	<3e-2(--)	0.087(0.013)	2.701(0.534)	51.2(38)	0.1762(0.2264)	-- (--)	1.20(0.52)	-- (--)
SP050313-1 II	-7	<4e-3(--)	0.2565(0.0210)	0.0144(0.0006)	<1e-3(--)	<4e-2(--)	0.028(0.002)	2.990(0.285)	39.3(3.4)	-- (--)	0.472(0.056)	-- (--)	-- (--)
SP020313-1 II	-6	<4e-3(--)	0.2254(0.0200)	0.0191(0.0008)	<5e-3(--)	<2e-2(--)	0.076(0.008)	1.948(0.124)	62.3(18)	-- (--)	-- (--)	-- (--)	-- (--)
SP130813-2 II	-3.4	<3e-3(--)	0.1715(0.0139)	0.0189(0.0008)	<2e-4(--)	<4e-2(--)	0.115(0.022)	0.679(0.036)	51.8(12)	-- (--)	0.767(0.092)	-- (--)	0.09(0.04)
SP020313-2 III	-7	<9e-3(--)	0.2144(0.0181)	0.0254(0.0011)	<9e-3(--)	<2e-2(--)	0.042(0.005)	3.562(0.159)	53.3(6.8)	-- (--)	-- (--)	-- (--)	-- (--)
SP220713-2 III	-6	<1e-3(--)	0.2269(0.0212)	0.0167(0.0007)	<1e-3(--)	-- (--)	0.199(0.051)	2.169(0.119)	57.9(7.6)	-- (--)	-- (--)	-- (--)	-- (--)
SP050313-4 III	-3.4	<2e-4(--)	0.2460(0.0209)	0.0177(0.0007)	<4e-4(--)	-- (--)	0.088(0.007)	0.393(0.017)	59.7(5.8)	-- (--)	0.862(0.194)	-- (--)	-- (--)
SP130813-4 IV	-7	<2e-2(--)	0.2446(0.0198)	0.0312(0.0014)	<2e-2(--)	<4e-2(--)	0.522(0.038)	3.257(0.153)	40.2(4.7)	-- (--)	-- (--)	-- (--)	0.20(0.08)
SP020313-3 IV	-6	<1e-3(--)	0.2216(0.0203)	0.0149(0.0006)	<8e-8(--)	<1e-2(--)	0.454(0.037)	1.805(0.093)	49.9(5.4)	-- (--)	0.460(0.131)	-- (--)	-- (--)
SP050313-2 IV	-3.4	-- (--)	0.2172(0.0175)	0.0117(0.0005)	-- (--)	-- (--)	0.478(0.038)	0.342(0.015)	47.0(4.9)	-- (--)	0.289(0.040)	0.023(0.008)	0.08(0.03)

Compositions: I = SM-20, II = SKHAND1-a, III = SKHAND1-b, IV = SKHAND1-c. Errors (1-sigma standard deviation) are given in parenthesis.

TABLE V (continuation)

Run	log fO₂	D(Na)	D(Mg)	D(Al)	D(K)	D(Ca)	D(Sc)	D(V)	D(Cr)	D(Mn)	D(Fe)	D(Co)	D(Ni)	D(U)
SP070713-4	I -12	12.9(4.3)	20.1(3.3)	-- (--)	<7e-4(--)	0.0057(0.0014)	7.60(0.57)	89.6(16)	<5e-4(--)	10.7(0.75)	164.2(79.6)	58.5(11)	0.0026(0.0017)	0.174(0.006)
SP220713-4	I -11	13.7(4.3)	13.5(3.4)	-- (--)	<1e-3(--)	0.0017(0.0005)	4.57(0.54)	55.7(4.0)	<6e-4(--)	7.16(1.17)	125.3(19.9)	36.6(6.8)	0.0015(0.0014)	0.126(0.003)
SP300713-3	I -10	14.8(3.9)	15.8(3.5)	-- (--)	<9e-4(--)	0.0022(0.0016)	5.73(0.34)	71.5(6.2)	<8e-4(--)	8.41(0.78)	206.7(43.7)	43.7(3.7)	0.0007(0.0001)	0.218(0.017)
SP070813-2	I -9	10.7(1.4)	14.3(2.0)	-- (--)	<5e-4(--)	0.0016(0.0007)	3.20(0.17)	47.5(11)	<1e-4(--)	4.77(0.22)	173.3(93.7)	24.9(3.2)	0.0006(0.0003)	0.181(0.031)
SP100813-5	I -8	14.7(2.2)	13.8(1.8)	-- (--)	<1e-2(--)	0.0150(0.0060)	5.08(0.27)	57.6(6.5)	<1e-3(--)	6.78(0.38)	129.0(36.0)	14.0(1.6)	0.0117(0.0059)	0.286(0.018)
SP050313-3	I -7	3.5(0.4)	3.7(0.5)	0.044(0.022)	<6e-4(--)	0.0010(0.0013)	2.19(0.16)	31.0(1.8)	<4e-4(--)	3.17(0.33)	171.4(45.1)	9.5(1.7)	0.0005(0.0003)	0.262(0.006)
SP020313-5	I -6	3.2(0.7)	4.5(0.7)	0.015(0.009)	<6e-4(--)	0.0008(0.0002)	1.60(0.08)	16.0(0.7)	<1e-4(--)	2.31(0.20)	44.1(9.1)	7.0(0.7)	0.0006(0.0009)	0.338(0.030)
SP270213-5	I -5	3.4(0.3)	6.1(0.6)	0.015(0.004)	<8e-4(--)	0.0018(0.0008)	1.68(0.04)	15.9(0.7)	<6e-4(--)	2.36(0.13)	58.8(14.5)	11.0(1.3)	0.0008(0.0003)	0.377(0.036)
SP130813-3	I -3.4	1.9(0.2)	2.8(0.4)	0.003(0.001)	<2e-4(--)	0.0009(0.0004)	1.29(0.08)	14.4(0.9)	<1e-4(--)	2.04(0.12)	100.9(20.3)	-- (--)	0.0007(0.0003)	0.166(0.010)
SP180213-5	I -3.4	0.8(0.1)	8.9(4.5)	0.013(0.010)	<2e-4(--)	0.0015(0.0011)	1.67(0.08)	12.7(1.4)	<2e-4(--)	2.50(0.17)	56.8(8.5)	8.1(0.9)	0.0009(0.0007)	0.420(0.044)
SP210213-5	I -2	1.2(0.2)	3.5(0.5)	0.015(0.002)	<4e-4(--)	0.0021(0.0001)	1.28(0.07)	11.0(0.4)	<3e-4(--)	1.80(0.12)	41.8(1.2)	10.0(1.3)	0.0011(0.0005)	0.293(0.009)
SP250713-4	I -0.7	0.9(0.1)	3.9(1.1)	0.023(0.004)	<9e-4(--)	0.0022(0.0008)	2.14(0.22)	22.5(2.8)	<8e-4(--)	3.09(0.26)	96.5(24.7)	17.3(1.5)	0.0011(0.0009)	0.945(0.035)
SP240213-5	I 0	0.2(0.1)	1.9(0.5)	0.012(0.007)	<2e-4(--)	0.0008(0.0004)	1.21(0.03)	10.6(0.5)	<1e-4(--)	1.70(0.05)	38.5(3.6)	7.6(0.6)	0.0003(0.0002)	0.286(0.012)
PC100813	I 4.3	0.13(0.0)	0.12(0.0)	0.025(0.008)	<2e-3(--)	0.0012(0.0002)	1.07(0.03)	7.4(0.2)	-- (--)	1.36(0.12)	16.2(0.7)	1.1(0.1)	0.0001(0.0001)	0.234(0.011)
SP220713-1	II -11	8.4(2.3)	11.4(2.5)	-- (--)	<1e-2(--)	0.0302(0.0129)	4.37(0.28)	19.5(1.3)	<1e-2(--)	5.08(0.33)	38.1(7.7)	4.0(1.1)	0.0856(0.0496)	0.026(0.002)
SP050313-1	II -7	5.0(0.4)	7.9(0.9)	-- (--)	<8e-4(--)	0.0052(0.0021)	3.56(0.19)	24.8(1.7)	<2e-3(--)	5.28(0.38)	83.6(42.7)	3.1(0.6)	0.1127(0.0565)	0.228(0.033)
SP020313-1	II -6	6.2(0.8)	11.4(1.7)	-- (--)	<9e-4(--)	-- (--)	3.25(0.18)	21.5(1.2)	<3e-3(--)	4.69(0.25)	79.8(16.3)	3.0(0.8)	0.0577(0.0292)	0.291(0.022)
SP130813-2	II -3.4	3.8(1.2)	14.6(2.8)	0.016(0.006)	<4e-4(--)	0.0174(0.0070)	3.97(0.22)	26.1(5.0)	<4e-3(--)	5.71(0.31)	90.5(27.7)	1.7(0.2)	0.0098(0.0049)	1.096(0.067)
SP020313-2	III -7	6.7(0.8)	7.2(1.1)	0.003(0.001)	<1e-2(--)	0.0256(0.0103)	3.66(0.18)	21.8(1.1)	<2e-2(--)	5.22(0.27)	101.9(21.9)	2.3(0.4)	0.0570(0.0286)	0.245(0.051)
SP220713-2	III -6	14.7(9.8)	9.4(4.0)	0.011(0.005)	<6e-4(--)	-- (--)	3.42(0.18)	20.8(1.1)	<5e-3(--)	4.95(0.26)	74.9(15.8)	3.8(0.8)	0.0303(0.0152)	0.267(0.018)
SP050313-4	III -3.4	4.8(0.9)	7.8(2.2)	0.106(0.043)	-- (--)	0.0151(0.00061)	2.92(0.15)	14.2(0.7)	-- (--)	4.49(0.23)	61.4(12.4)	0.8(0.1)	0.0452(0.0228)	0.263(0.019)
SP130813-4	IV -7	5.9(0.7)	6.8(1.0)	0.086(0.035)	<1e-3(--)	0.0218(0.0087)	3.96(0.23)	29.8(2.6)	<2e-2(--)	6.23(0.38)	93.4(23.1)	9.4(1.1)	0.0190(0.0095)	0.577(0.036)
SP020313-3	IV -6	7.5(1.9)	22.0(6.7)	0.093(0.038)	<1e-3(--)	0.0036(0.0014)	3.45(0.19)	30.0(2.7)	<8e-4(--)	4.87(0.56)	80.9(20.0)	9.9(2.9)	0.0042(0.0021)	0.634(0.051)
SP050313-2	IV -3.4	4.0(0.7)	10.2(2.3)	0.089(0.036)	<7e-4(--)	0.0016(0.00007)	2.95(0.16)	22.8(1.7)	-- (--)	4.29(0.56)	77.3(16.2)	3.0(0.3)	-- (--)	0.690(0.050)

Compositions: I = SM-20, II = SKHAND1-a, III = SKHAND1-b, IV = SKHAND1-c. Errors (1-sigma standard deviation) are given in parenthesis.

with composition SM20. In order to separate these two effects, we fitted the partitioning data obtained for quadrivalent homovalent cations (Zr^{4+}, Hf^{4+}, Ti^{4+} and Th^{4+}) for each individual experiment with composition SM20 to the lattice strain model of Blundy and Wood (1994), and then extracted a theoretical estimate for the partitioning of V^{4+} by taking its ionic radius in VI-fold coordination and substituting it into the Blundy and Wood's equation. The results are illustrated in Fig. 9, and show that at low oxygen fugacity, the measured partition coefficients of V agree well with the modeled parabola for the other quadrivalent element, but as fO_2 conditions increase, the partition coefficients become progressively smaller. Taking the difference between the theoretically calculated partition coefficient for V^{4+} (determined by the lattice strain fits) and the measured V partition coefficient and plotting these values as a function of oxygen fugacity, we could then evaluate the sole effect of oxygen fugacity on the vanadium rutile/silicate partitioning (Fig. 10). The results show a relatively constant value from log fO_2 of 0 up to -7, and then a pronounced increase towards more reducing conditions. The transition is better fitted with a slope of 0.25 rather than 0.5, indicating a 1-electron redox processes and therefore a change from V^{4+} to V^{5+} (see Mallmann and O'Neill 2009 for a theoretical background). Surprisingly, even at the most reducing conditions, there is no indication for the presence of V^{3+} in our rutile/silicate partitioning experiments.

Other well-known heterovalent elements included in our study for which we were able to collect data are Cr, Fe, W and U. Results obtained for composition SM20 are plotted as a function of oxygen fugacity in Fig. 7b. Tungsten gives relatively constant partition coefficients (~ 9) from log fO_2 of 0 to -7, which are interpreted as reflecting W^{6+} based on recent results obtained by Fonseca et al. (2014) for other phases, and then shows a constant increase from about log fO_2 of -7 towards reducing conditions, likely due to the presence of small amounts of W^{4+}. The partition coefficient obtained for W at log fO_2 of +4.3 is almost an order of magnitude lower, which
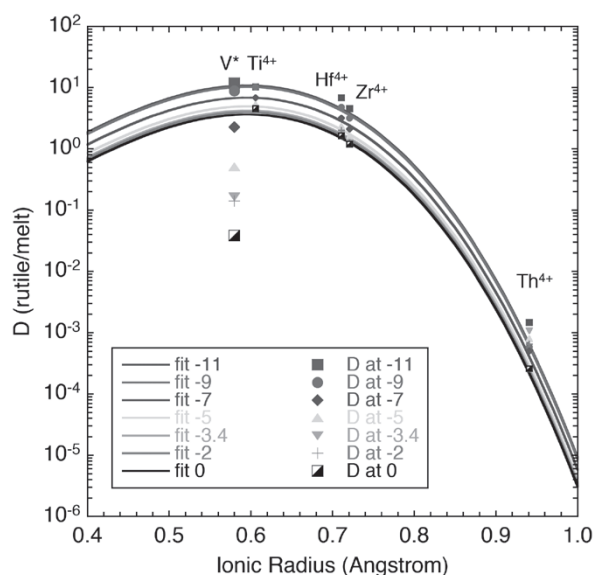

Figure 9 - Partition coefficients of quadrivalent cations and vanadium between rutile and silicate melt plotted as a function of ionic radius in VI-fold coordination. The lines are best fits for quadrivalent cations to the lattice strain model (Equation 2 of Blundy and Wood, 1994). Ionic radius taken from Shannon (1976), with assumed uncertainty of 0.002 Å. Error bars are not shown for clarity.

could indicate a significant pressure effect on W partitioning since this experiment was carried out at a pressure of 1 GPa. Iron behaved as would be expected for an element with transition from 2+ to 3+ valence states, with partitioning data plotting along a sigmoidal-shaped function of slope of 0.25 with a plateau at the oxidizing end defining the partitioning of Fe^{3+} as ~ 0.1, and a plateau at the reducing end defining the partitioning of Fe^{2+} as ~ 0.026. Chromium, with expected transition from 2+ to 3+ (Berry and O'Neill 2004), and uranium, with expected transition from 4+ to 5+ to 6+ (Berry et al. 2008), do not show a clear trend with oxygen fugacity. This may be due to the superimposed effects of oxygen fugacity and melt composition.

PARTITIONING OF HOMOVALENT ELEMENTS

Partitioning data for a number of homovalent trace element cations were determined. Among the trivalent cations, Sc is the least incompatible
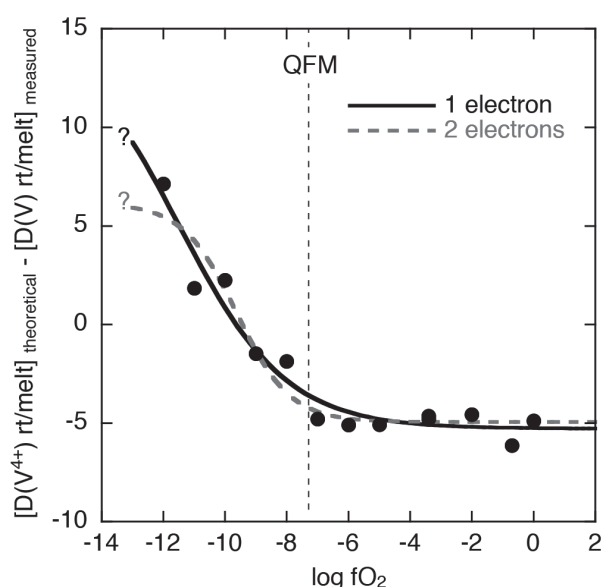
Figure 10 - Absolute difference between partitioning coefficients calculated for V^{4+} using the lattice strain model fits to other quadrivalent cations (see Figure 6) and the measured partition coefficients for V between rutile and silicate melt plotted against oxygen fugacity. The lines are best fits of the data to an equation of the same functional form as Equation 15 in Mallmann and O'Neill (2007), assuming a redox transition between 1 electron (fO_2 raised to the coefficient of 0.25; solid line) and 2 electrons (fO_2 raised to the coefficient of 0.5; dashed line). QFM refers to the quartz-fayalite-magnetite buffer at 1300°C and 1 bar.

(average Ds ~ 0.36), followed by Al and Ga (average Ds ~ 0.02) and then Y (average Ds ~ 0.003), although there is a systematic change with composition, with Ds increasing by a factor of 4 with increasing melt polymerization. Among the divalent cations, Cu and Zn are compatible and strongly affected by melt composition, with Ds ranging from about unity to 10-20 as melt polymerization increases. All the other divalent cations (Mg, Ca, Mn, Co, Ni and Sr) give Ds < 0.1. All monovalent cations (Na, Ba, K) are highly incompatible in rutile, and their partition coefficients should be seen as maximum due to the potential contamination of rutile LA-ICP-MS analyses with melt inclusions. The HFSEs are all compatible in rutile, with partition coefficients for Zr (1.1-7.6), Hf (1.4-10.7), Nb (7.4-90) and Ta (16-206) showing a range that is in agreement

with previous experimental studies (see Figure 1 in Klemme et al. 2005). The absolute values, however, vary quite significantly with melt composition. In particular, there is an increase in Ds for all HFSEs from less to more polymerized melts (Fig. 8). We did not observe, however, any systematic difference in HFSEs partition coefficients determined for experiments with compositions SKHDAN1a, b and c. In other words, the type of trace element doping appears to have no effect on HFSE incorporation into rutile. Finally, as previously reported by Klemme et al. (2005), ($D = 10^{-5} - 10^{-3}$) is at least 2 orders of magnitude more incompatible in rutile than ($D = 0.12 - 1.1$).

SOME PETROLOGICAL IMPLICATIONS

As previously noted in other experimental studies, melt composition has a strong effect on the partitioning of HFSE between rutile and silicate melt. Rutile/melt partition coefficients increase with increasing melt polymerization. Linear regressions of our experimental data at 1-bar for compositions SM20 and SKHDAN1 give (Fig. 8):

$$D_{Zr}^{Rt/melt} = -109\Lambda + 65 \ (r^2 = 0.76)$$
$$D_{Nb}^{Rt/melt} = -1187\Lambda + 703 \ (r^2 = 0.92)$$
$$D_{Hf}^{Rt/melt} = -155\Lambda + 93 \ (r^2 = 0.75)$$
$$D_{Ta}^{Rt/melt} = -3091\Lambda + 1856 \ (r^2 = 0.70)$$

where Λ is the optical basicity of the melt as defined by Duffy (1993). Hence, the amount of HFSE that can be incorporated (or retained) in rutile will be strongly dependent on the composition of the partial melts.

An interesting result of this study is the fact that Ta and Nb, both with valence 5+, are more compatible in rutile than Zr and Hf, which have valence 4+ and therefore do not require charge balance to substitute for Ti^{4+} in rutile. This indicates that the most important factor in the incorporation of trace elements in mineral phases is the size of the cation rather than its charge, since Ta^{5+} and Nb^{5+}

both have ionic radii in octahedral coordination closer to Ti^{4+} than Zr^{4+} and Hf^{4+}. In this connection, our results do not indicate any change in HFSE partition coefficients due to the presence of other trace elements, as evidenced by results obtained with composition SKHDAN1 doped with different cocktails of trace elements.

Finally, Th is about 2 orders of magnitude more incompatible than U in rutile, a result that may have implications for interpreting U-series disequilibria, particularly because U is a heterovalent element and Th is not.

RESUMO

Magmas produzidos em zonas de subducção possuem um característico empobrecimento em elementos de elevado potencial de ionização (HFSE) em comparação com outros elementos de incompatibilidade similar. Essa assinatura geoquímica pode ser atribuída a presença do mineral acessório rutilo (TiO_2) como fase residual. Dados experimentais obtidos nesse estudo mostram que o coeficiente de partição de vanádio entre rutilo e líquidos silicáticos varia entre ~0,1 (incompatível) e ~18 (compatível) em função da fugacidade de oxigênio. Os resultados experimentais confirmam ainda que HFSE são compatíveis em rutilo, com coeficientes de partição (D) para Ta > Nb >> Hf > /~ Zr, porém fortemente dependentes da composição do líquido silicático. Coeficientes de partição para HFSE aumentam aproximadamente uma ordem de magnitude com aumento do grau de polimerização do líquido silicático (ou decréscimo da basicidade). Os resultados experimentais também indicam que a presença de rutilo como fase acessória residual pode resultar no fracionamento de U relativo a Th devido a diferença (~ duas ordens de magnitude) entre os coeficientes de partição desses dois elementos. Também confirma-se com os resultados desse estudo que além dos HFSE, Cr, Cu, Zn e W são compatíveis em rutilo em qualquer fugacidade de oxigênio.

Palavras-chave: magmas de arco, elementos de elevado potencial de ionização, coeficientes de partição, redox, rutilo.

REFERENCES

BELONOSHKO A AND SAXENA SK. 1991. A molecular dynamics study of the pressure-volume-temperature properties of supercritical fluids: II. CO_2, CH_4, CO, O_2 and H_2. Geochim Cosmochim Acta 55: 3191-3208.

BERRY AJ AND O'NEILL HStC. 2004. A XANES determination of the oxidation state of chromium in silicate glasses. Am Mineral 89: 790-798.

BERRY AJ, O'NEILL HStC AND FORAN GJ. 2008. The oxidation state of uranium in mantle melts. Goldschmidt Conference, Abstract. Geochim Cosmochim Acta 72: A79-A79.

BLUNDY J AND WOOD B. 1994. Prediction of crystal-melt partition coefficients from elastic moduli. Nature 372: 452-454.

BRENAN JM, SHAW HF, RYERSON FJ AND PHINNEY DL. 1995. Mineral-aqueous fluid partitioning of trace elements at 900°C and 2.0 GPa – Constraints on the trace element chemistry of mantle and deep crustal fluids. Geochem Cosmochim Acta 59: 3331-3350.

COTTRELL E AND KELLEY KA. 2011. The oxidation state of Fe in MORB glasses and the oxygen fugacity of the upper mantle. Earth Planet Sci Lett 305: 270-282.

DUFFY FA. 1993. A review of optical basicity and its applications to oxidic systems. Geochim Cosmochim Acta 57: 3961-3970.

EVANS KA. 2012. The redox budget of subduction zones. Earth Sci Rev 113: 12-32.

FONSECA ROC, MALLMANN G, SPRUNG P, SOMMER JE, HEUSER A, SPEELMANNS IM AND BLANCHARD H. 2014. Redox controls on tungsten and uranium crystal/silicate melt partitioning and implications for the W/U and Th/U ratio of the lunar mantle. Earth Planet Sci Lett 404: 1-13.

GREEN TH AND PEARSON NJ. 1987. An experimental study of Nb and Ta partitioning between Ti-rich minerals and silicate minerals at high pressure and temperature. Geochim Cosmochim Acta 51: 55-62.

HORGN WS AND HESS PC. 2000. Partition coefficients of Nb and Ta between rutile and anhydrous haplogranite melts. Contrib Mineral Petrol 138: 176-185.

IONOV DA AND HOFMANN AW. 1995. Na-Ta-rich mantle amphiboles and micas: Implications for subduction related metasomatic trace element fractionation. Earth Planet Sci Lett 131: 341-356.

Jоchum KP et al. 2011. Determination of reference values for NIST SRM 610-617 glasses following ISO guidelines. Geost Geoanal Res 35: 397-429.

Kelley KA and Cottrell E. 2009. Water and the oxidation state of subduction zone magmas. Science 325: 605-607.

Keppler H. 1996. Constraints from partitioning experiments on the composition of subduction zone fluids. Nature 380: 237-240.

Klemme S, Prowartke S, Hametner K and Gunther D. 2005. Partitioning of trace elements between rutile and silicate melts: Implications for subduction zones. Geochim Cosmochim Acta 69: 2361-2371.

Kress V, Ghiorso M and Lastuka C. 2004. Microsoft EXCEL spreadsheet-based program for calculating equilibrium gas speciation in the COHS-Cl-F system. Comput Geosci 30: 211-214.

Mallmann G and O'Neill HStC. 2007. The effect of oxygen fugacity on the partitioning of Re between crystals and silicate melt during mantle melting. Geochim Cosmochim Acta 71: 2837-2857.

Mallmann G and O'Neill HStC. 2009. The crystal/melt partitioning of V during mantle melting as a function of oxygen fugacity compared with some other elements (Al, P, Ca, Sc, Ti, Cr, Fe, Ga, Y, Zr and Nb). J Petrol 50: 1765-1794.

Mallmann G and O'Neill HStC. 2013. Calibration of an empirical thermometer and oxybarometer based on the partitioning of Sc, Y and V between olivine and silicate melt. J Petrol 54: 933-949.

McCulloch MT and Gamble JT. 1991. Geochemical and geodynamical constraints on subduction zone magmatism. Earth Planet Sci Lett 102: 358-374.

Mills KC. 1993. The influence of structure on the physicochemical properties of slags. ISIJ International 33: 148-155.

Rudnick RL, Barth M, Horn I and McDonough W. 2000. Rutile bearing refractory eclogites: Missing link between continents and depleted mantle. Science 287: 278-281.

Shannon RD. 1976. Revised effective ionic radii and systematic studies of interatomic distances in halides and chalcogenides. Acta Crystallog Section A 32: 751-767.

Stalder R, Foley SF, Brey GP and Horn I. 1998. Mineral aqueous fluid partitioning of trace elements at 900-1200°C and 3.0-5.7 GPa: New experimental data for garnet, clinopyroxene, and rutile, and implications for mantle metasomatism. Geochim Cosmochim Acta 62: 1781-1801.

Tatsumi Y and Eggins S. 1995. Subduction zone magmatism. Frontiers in Earth Science Series, 1st Edition, Blackwell, Cambridge, USA.

Tiepolo M, Vannucci R, Oberti R, Foley S, Bottazzi P and Zanetti A. 2000. Nb and Ta incorporation and fractionation in titanian pargasite and kaersutite: Crystal chemical constraints and implications for natural systems. Earth Planet Sci Lett 176: 185-201.

Zack T, Kronz A, Foley S and Rivers T. 2002. Trace element abundances in rutile from eclogites and associated garnet mica schists. Chem Geol 184: 97-122.